Including high frequency variability in coastal ocean acidification projections

Yuichiro Takeshita*[1,2], Christina A. Frieder[1,3], Todd R. Martz[1], John R. Ballard[1], Richard A. Feely[4], Susan Kram[1], SungHyun Nam[1,5], Michael O. Navarro[1,6], Nichole N. Price[1,7], and Jennifer E. Smith[1]

1. Scripps Institution of Oceanography, University of California San Diego, La Jolla, CA 92093
2. now at: Carnegie Institution for Science, Stanford, CA 94305
3. now at: University of Southern California, Los Angeles, CA 90089
4. Pacific Marine Environmental Laboratory, NOAA, Seattle, WA 98115, USA
5. now at: Research Institution of Oceanography/School of Earth and Environmental Sciences, Seoul National University, Seoul 151-742, Republic of Korea
6. now at: California State University Monterey Bay, Seaside, CA 93955, USA
7. now at: Bigelow Laboratory for Ocean Sciences, East Boothbay, ME 04544

* Corresponding Author: Carnegie Institution for Science, Department of Global Ecology, Stanford, CA 94305 (ytakeshita@carnegiescience.edu)

Keywords: ocean acidification, acidification projection, pCO_2, upwelling margins, near-shore habitats, calcium carbonate saturation state

Running Head: Unique Habitat Acidification Projections

Abstract

Assessing the impacts of anthropogenic ocean acidification requires knowledge of present-day and future environmental conditions. Here, we present a simple model for upwelling margins that projects anthropogenic acidification trajectories by combining high-temporal resolution sensor data, hydrographic surveys for source water characterization, empirical relationships of the CO_2 system, and the atmospheric CO_2 record. This model characterizes CO_2 variability on timescales ranging from hours (e.g. tidal) to months (e.g. seasonal), bridging a critical knowledge gap in ocean acidification research. The amount of anthropogenic carbon in a given water mass is dependent on the age, therefore a density-age relationship was derived for the study region, and was combined with the 2013 Intergovernmental Panel on Climate Change CO_2 emission scenarios to add density-dependent anthropogenic carbon to the sensor time series. The model was applied to time series from four autonomous pH sensors, each deployed in the surf zone, kelp forest, submarine canyon edge, and shelf break in the upper 100 m of the Southern California Bight. All habitats were within 5 km of one another, and exhibited unique, habitat-specific CO_2 variability signatures and acidification trajectories, *demonstrating the importance of making projections in the context of habitat-specific CO_2 signatures*. In general, both the mean and range of pCO_2 increase in the future, with the greatest increases in both magnitude and range occurring in the deeper habitats due to reduced buffering capacity. On the other hand, the saturation state of aragonite (Ω_{Ar}) decreased in both magnitude and range. This approach can be applied to the entire California Current System, and upwelling margins in general, where sensor and complementary hydrographic data are available.

1 Introduction

It has become increasingly apparent that upwelling systems, including the California Current System (CCS), are particularly vulnerable to anthropogenic ocean acidification due to their unique physical and chemical traits (Feely et al., 2008, 2010; Gruber et al., 2012; Hauri et al., 2013a, 2013b). Upwelled waters have been isolated from the atmosphere and are naturally elevated in CO_2 from remineralization of organic matter; depending on the age of the upwelled water mass it may also contain anthropogenic carbon (Harris et al., 2013; Sabine et al., 2002). Recent observations estimate the saturation horizon with respect to aragonite (depth at which $\Omega_{Ar} = 1$) along the CCS has shoaled by approximately 50 m since preindustrial times, and undersaturated waters ($\Omega_{Ar} < 1$) have been observed at the surface near the California-Oregon border during a strong upwelling event (Alin et al., 2012; Feely et al., 2008; Harris et al., 2013). Furthermore, the rate of acidification (i.e. ΔpH yr^{-1}) is expected to be significantly higher along upwelling margins than observed in the surface open ocean (Bates et al., 2014; Gruber et al., 2012; Hauri et al., 2013b; Leinweber and Gruber, 2013; Rykaczewski and Dunne, 2010) due to the reduced buffering capacity of seawater at higher levels of CO_2 (Frankignoulle, 1994). This effect has caused parts of the CCS to venture beyond the envelope (defined as: mean ± 1 s.d.) from modeled preindustrial Ω_{Ar} conditions (Hauri et al., 2013b). This is a concern because organisms may need to survive outside of the environmental conditions to which they are acclimatized, and the evolutionary potential for key ecological species to adapt to such rapid and unprecedented changes is poorly understood. For example, a significant decrease in calcareous benthic organisms was observed along a natural pH gradient near a cold volcanic CO_2 vent (Hall-Spencer et al., 2008; Kroeker et al., 2011). However, some calcareous organisms such as limpets seemed to have adapted to higher CO_2 levels compared to corals and mussels in the same

system (Rodolfo-Metalpa et al., 2011). Furthermore for upwelling margins, CO_2 co-varies with other environmental stressors such as temperature and O_2 (Reum et al., 2015), making predictions more difficult due to potential non-linear synergistic effects (Frieder et al., 2014).

A critical component in making accurate impact assessments of ocean acidification is the development of robust, ecosystem-specific projections of future CO_2 conditions (Andersson et al., 2013; Cai et al., 2011; Feely et al., 2009, 2010; McNeil and Matear, 2008; Sunda and Cai, 2012). Development of surface, open-ocean acidification projections has been relatively straightforward, as they rely on well-defined chemical principles of CO_2 equilibrium at the air-sea interface (Byrne et al., 2010; Lauvset and Gruber, 2014). Models become more complicated when attempting to resolve biological and physical processes that contribute significantly to the natural variability of the system. For example, biologically mediated "enhanced acidification" was identified in the northern Gulf of Mexico, causing significantly faster rates of acidification than the open ocean (Cai et al., 2011). On many tropical coral reefs, seasonal patterns in CO_2 are minimal, whereas the dominant frequency of variability occurs on diel and tidal frequencies (Hofmann et al., 2011). On upwelling margins, both biological and physical processes contribute to the observed natural variability of carbonate conditions (Fassbender et al., 2011).

One approach to develop region-specific ocean acidification projections is to apply an eddy-resolving regional ocean model system (ROMS) coupled with a biogeochemical component, as has been developed for the CCS (Gruber et al., 2011, 2012; Hauri et al., 2013b). Such models have highlighted the importance of capturing physical and biological processes in highly dynamic upwelling systems. The model simulations show complex spatiotemporal variability (Hauri et al., 2013b), and predict that the frequency of "corrosive" upwelling events will intensify in both magnitude and duration by the year 2050 (Hauri et al., 2013a). However,

92 the eddy-resolving ROMS project pCO_2 and saturation state conditions on a 5-km grid, whereas
93 many marine animals experience the environment on the scale of centimeters to meters. In
94 addition, regional models can largely resolve event-scale (weeks) and seasonal features, but
95 cannot capture fluctuations on diel to tidal time scales, which can be the dominant frequency of
96 variability in many near-shore environments (Duarte et al., 2013; Frieder et al., 2012; Hofmann
97 et al., 2011). Due to this discrepancy in both space and time, numerical models tend to
98 underestimate or entirely miss the high-frequency variability that exists for the microclimate of
99 organisms.

100 To transition from region-specific to habitat-specific ocean acidification projections, high
101 temporal resolution data from autonomous chemical sensors deployed across many habitat types
102 can be used to directly quantify the full range of present-day carbonate conditions (Harris et al.,
103 2013; Hofmann et al., 2011, 2014; Martz et al., 2014; Sutton et al., 2014). The CCS supports
104 many ecosystems that are of great ecological and economic value. In particular, there is great
105 habitat and species diversity near-shore on the shelf, which includes a large number of
106 commercially important invertebrates and fishes. Habitats in the region include bays and
107 estuaries, rocky and sandy intertidal, eelgrass beds and kelp forests, sub-tidal reefs, canyons and
108 extensive sandy sea floor. There are many endangered and harvested benthic organisms that
109 inhabit only one or a subset of these habitats.

110 Sensor data provide key observations for the mechanistic understanding of the controls
111 on environmental conditions, and are particularly needed for coastal marine environments where
112 complex physical and biological processes influence the observed variability. For example,
113 sensor data from a near-shore kelp forest in the southern CCS revealed that local biological
114 feedbacks and episodic upwelling events were the dominant drivers of CO_2 variability, with

115 pCO_2 fluctuating by 600 µatm at 17-m water depth (Frieder et al., 2012). This scale of variability
116 associated with near-shore environments is not captured by regional model simulations, but is
117 most relevant for organisms living inside the kelp forest.

118 Here, we present an anthropogenic ocean acidification model to project CO_2 chemistry
119 into the future by combining autonomous chemical sensor data, regional empirical relationships
120 for the CO_2 system (Alin et al., 2012), hydrographic data, and the atmospheric CO_2 record
121 (Keeling et al., 2005). This model was applied to four habitats ranging from the surface to 100-m
122 water depth and all within 5 km of each other in the Southern California Bight (SCB). Each site
123 showed distinct CO_2 variability signatures and acidification trajectories, highlighting the
124 importance of interpreting ocean acidification projections in the context of present and future
125 habitat-specific CO_2 signatures. Implications for future ocean acidification research are discussed.

126 **2 Methods**

127 *2.1 Study Sites*

128 Moored autonomous sensor packages SeapHOx or SeaFET (Bresnahan et al., 2014) were
129 deployed at four depths (4, 17, 30, and 88 m) within several distinct habitats on the San Diego
130 continental shelf for 1 year starting June 2012 (Figure 1). All sensors were deployed near the
131 seafloor; the three shallowest sensors were deployed within 3 m of the bottom, and the deepest
132 sensor was moored 12 m above the seafloor (Table 1).

133 A SeaFET was deployed at the Ellen Browning Scripps Pier 2 m above the benthos as a
134 part of the Scripps Ocean Acidification Real-time Monitoring Program. The sensor was located
135 approximately 400 m from the shore in the surf zone. Weekly discrete samples for total alkalinity
136 (TA) and dissolved inorganic carbon (DIC) were taken alongside the sensors for calibration and

quality control following standard protocols (Dickson et al., 2007). The sensor was serviced every 1-2 months to remove biofouling organisms.

The La Jolla kelp forest is part of the South La Jolla State Marine Reserve and is characterized by a dense population of *Macrocystis pyrifera*. The chemical variability in this ecosystem is strongly influenced by regional physical processes (*e.g.*, upwelling and stratification) and local biological feedbacks (*e.g.*, production and respiration). A SeapHOx was deployed at 17 m in the southern portion of the kelp forest, 3 m above the bottom. The reader is referred to *Frieder et al.*, 2012 for further details on site and deployment description.

The La Jolla canyon is a submarine canyon plunging from approximately 20 m to a depth of 1000 m within several km from shore. A SeapHOx was deployed over a sandy bottom at the southern canyon edge at 30 m depth within the Matlahuayl state marine reserve; the O_2 sensor malfunctioned and thus is not included. The water in the La Jolla canyon is characterized by higher salinity, and lower temperature, O_2, and pH (data not shown). Tidal energy in submarine canyons is significantly amplified (Swart et al., 2011), bringing deep water from the canyon to the canyon edge. Therefore, physical forcings are the dominant drivers for chemical variability at this site (Navarro et al., 2013).

The Del Mar Buoy was first deployed in 2006 at 100 m off of Del Mar in northern San Diego at the shelf break, and has provided continuous time series data (e.g. temperature, salinity, oxygen, and current) at discrete depths (Frieder et al., 2012; Send and Nam, 2012). A SeaFET sensor was deployed on the mooring at 88 m in 2011, and has provided a near-continuous time series of pH since. Co-located sensors include temperature, salinity (SBE 37), and dissolved oxygen (O_2; Aanderaa Optode). Water at this depth is isolated from the atmosphere and below the euphotic zone, and thus influenced primarily by upwelling and tidal dynamics.

2.2 Cruise data

Hydrographic data were collected aboard R/V Melville during the student-led San Diego Coastal Expedition cruises in June/July and December of 2012 (Figure 1). The SCB is characterized by relatively weak (compared to the northern CCS), but nearly year-round upwelling. However, there is a clear seasonal cycle based on climatological data, where upwelling intensifies generally between April and August, with the maximum occurring in May (Bograd et al., 2009). The cruises therefore corresponded with upwelling (June/July) and non-upwelling (December) seasons. Water samples were collected at stations ranging from >100 km from shore at 1200 m water depth, to within 5 km from shore at 30 m depth. Discrete samples were analyzed for O_2, pH, and DIC; duplicate samples were collected during every cast.

Discrete samples for O_2 were collected and analyzed by titration using a custom-built system (Martz et al., 2012). The titrant was standardized prior to and after each cruise using KIO_3 standard solutions prepared in house (Fisher, lot 105595); no detectable drift was observed for either cruise. Precision was ± 0.6 μmol kg^{-1} (duplicate n = 62, 1 s.d.), and the accuracy was estimated to be ± 0.5% because KIO_3 standards were not recrystallized (Emerson, 1999).

Samples for DIC and pH were collected in 150-ml or 250-ml Pyrex serum bottles (13-mm neck) following standard procedures (Dickson et al., 2007). However, rather than leaving headspace, the bottle was filled completely, and a gray butyl stopper was inserted to prevent gas exchange and samples were analyzed within 4 hours of collection.

DIC samples were analyzed using custom-built system based on an infrared analyzer (LI-COR 7000) similar to systems built by others (Friederich et al., 2002; O'Sullivan and Millero, 1998). The DIC measurements were calibrated using Certified Reference Materials provided by the Dickson Lab at SIO, by applying a gain correction (slope) and assuming an offset of zero

(intercept). The reference materials were stored in CO_2 impermeable bags (3 L Scholle DuraShield®), and were measured frequently throughout the cruise. The stability of the reference material in the bag was verified by daily measurements of a new bottle; no drift was observed. Precision and accuracy of the DIC measurements were ± 2.5 µmol kg^{-1} (duplicate n = 67, 1 s.d.).

Samples for pH were analyzed spectrophotometrically at 20 °C (Clayton and Byrne, 1993) using an automated system (Carter et al., 2013). The pH is reported on the total hydrogen ion concentration scale. The indicator dye (m-cresol purple, ACROS Lot A0264321) was used as received from the manufacturer without further purification. An offset was applied based on measurements in certified Tris buffer provided by the Dickson Lab. The precision and accuracy of the measurements were estimated to be ± 0.0015 (duplicate n = 86, 1 s.d.) and ± 0.02 (Liu et al., 2011), respectively. TA and pCO_2 were calculated using CO2SYS (van Heuven et al., 2011) using pH and DIC as inputs, and carbonic acid dissociation constants from *Mehrbach et al.*, 1973 refit by *Lueker et al.*, 2000.

2.3 Sensor Data

The SeapHOx and SeaFET sensor packages utilize a modified Honeywell Durafet III pH combination electrode for high-frequency pH measurements (Martz et al., 2010). These sensor packages have been successfully deployed in ecosystems worldwide (Frieder et al., 2012; Hofmann et al., 2011; Kroeker et al., 2011; Martz et al., 2014; Price et al., 2012), and have been shown to have excellent stability in seawater for months to years (Bresnahan et al., 2014). The SeapHOx is an integrated sensor package that also consists of an Aanderaa 3835 oxygen optode, and a Seabird SBE 37 Conductivity-Temperature sensor all plumbed into a pumped flow stream;

205 the SeaFET measures pH using a passively flushed cell. Sampling frequencies were 1 hr^{-1} or
206 greater at all depths.

207 All pH measurements were calibrated based on discrete TA and DIC samples taken
208 alongside the sensor, at minimum at the beginning and end of each sensor deployment (n > 4 for
209 every site), as recommended by the best practices (Bresnahan et al., 2014). The resolution of the
210 pH measurements is better than 0.0005 pH, stability is estimated to be better than 0.005, and
211 accuracy is estimated to be ± 0.015. Sensors were removed periodically for maintenance, but all
212 were deployed for > 50 days during both the upwelling and relaxation season.

213 At the surf zone (surface waters), a constant TA value of 2240 µmol kg^{-1} was assumed,
214 since discrete TA samples showed low variability (2240 ± 7 (1 s.d.) µmol kg^{-1}, n = 57). For the
215 three subsurface sensors, TA was estimated (TA^{est}) using a regional empirical relationship
216 developed for the CCS, with temperature and salinity as inputs (Alin et al., 2012); an offset of +8
217 µmol kg^{-1} was applied to TA^{est} based on comparisons to discrete samples collected (root mean
218 squared error (RMSE) = 6 µmol kg^{-1}, n = 25). This offset was a persistent feature over multiple
219 years (2010 – 2012), thus most likely reflecting a regional surface TA influence that is not
220 incorporated in the empirical relationship developed for the whole CCS. DIC, pCO_2, and Ω_{Ar}
221 were calculated using CO2SYS (van Heuven et al., 2011) using pH sensor data and TA^{est} as
222 inputs. Uncertainty for the calculated DIC, pCO_2, and Ω_{Ar} is pH-dependent, but on average is
223 estimated to be ± 13 µmol kg^{-1}, ± 25 µatm, and ± 0.04, respectively. Daily range of sensor data
224 was calculated by first high-pass filtering the data with a 36 hour window, and then taking the
225 difference between the daily maximum and minimum. The mean daily range was then calculated
226 by averaging the resultant time series.

2.4 Modelling Future Carbonate Chemistry

2.4.1 Approach

The carbonate conditions were modeled by decreasing or increasing DIC while using TA conditions from 2012. Modeled projections were made for preindustrial times and for year t, where t ranges between 2012 and 2100. The model presented here is based on the ΔC_t^* approach (Gruber et al., 1996), but instead of using tracers to estimate the age of the water mass (e.g. CFC's), we used the atmospheric CO_2 record as a quasi-age tracer. The age of the water mass ranged between 0 and 50 years in this study region. Although this approach must be used with caution, we demonstrate that our estimates are in good agreement with previously published anthropogenic carbon inventory estimates using age tracer measurements in this region (Feely et al., 2008; Sabine et al., 2002). In this model, it was assumed that ocean acidification is due to anthropogenic CO_2 invasion through the air-sea interface alone. We also assumed that both the path of a particular water mass between the subduction and upwelling site and the rate of remineralization processes remain unchanged. Sensitivity to these assumptions is explored in the Discussion.

The DIC of the modeled year t (DIC_t) is calculated by

$$DIC_t = DIC_{2012} + \Delta DIC_{anth} \quad (1)$$

where DIC_{2012} is the DIC observed in 2012, and ΔDIC_{anth} is the additional anthropogenic CO_2 that the water mass would have absorbed since 2012. Different formulations for ΔDIC_{anth} were used for surface waters (i.e., above the seasonal mixed layer depth, defined here as $\sigma_\theta \leq 25.2$ kg m^{-3}) and subsurface waters ($\sigma_\theta > 25.2$ kg m^{-3}), and are outlined below.

For surface waters, ΔDIC_{anth} was calculated as the difference in surface DIC between year t and 2012. Surface DIC was calculated by assuming atmospheric equilibrium with TA =

249 2240 µmol kg^{-1} (based on water samples from the Scripps pier) and using $pCO_{2,atm}$ projection
250 under the 2013 IPCC RCP6.0 scenario (Hijioka et al., 2008). Although large deviations from
251 equilibrium conditions are often observed in the coastal ocean due to upwelling and biological
252 production (Hales et al., 2005), the mean pCO_2 calculated from sensor data at the surf zone was
253 394 ± 43 (1 s.d.) µatm (Table 2), suggesting that the surface water at the study site was near
254 atmospheric equilibrium.

255 For subsurface waters, ΔDIC_{anth} was quantified as the increase in DIC due to
256 anthropogenic CO_2 when the water parcel was last in contact with the atmosphere. The mass
257 balance of DIC for subsurface waters is:

$$DIC = DIC° + \Delta DIC_{bio} \quad (2)$$

258 where $DIC°$ is the preformed DIC, and ΔDIC_{bio} is the DIC added by remineralization processes
259 in the ocean interior. $DIC°$ can be expressed as the sum of DIC if it were in equilibrium with the
260 atmosphere (DIC_{eq}) and the degree of air-sea disequilibrium due to slow gas exchange kinetics
261 and biological processes (ΔDIC_{diseq}):

$$DIC° = DIC_{eq} + \Delta DIC_{diseq} \quad (3)$$

262 Since anthropogenic CO_2 only enters the ocean at the surface, the increase in DIC_{eq} represents
263 the anthropogenic ocean acidification signal, ΔDIC_{anth}, assuming ΔDIC_{diseq} is invariant with time.
264 However, in order to use this approach, the age of the water parcel must first be quantified, as
265 this determines the $pCO_{2,atm}$ with which it was last in contact.

266 The age of the water parcel was established by combining equations (2) and (3):

$$DIC_{eq}^{2012-age} = DIC - \Delta DIC_{bio} - \Delta DIC_{diseq} \quad (4)$$

where the superscript denotes the year at which the water parcel was last at the surface (i.e. equal to 2012 – age of the water mass). The age of the water mass was calculated by comparing the atmospheric CO_2 record to the $pCO_{2,atm}$ that is necessary to generate $DIC_{eq}^{2012-age}$. ΔDIC_{diseq} was estimated from published values in the region (Section 2.4.3). Using this information, we calculated ΔDIC_{anth} by:

$$\Delta DIC_{anth} = DIC_{eq}^{t-age} - DIC_{eq}^{2012-age} \quad (5)$$

where the superscripts denote the year at which the water parcel was last at the surface, and age is the age of the water parcel. For example, if age = 30 yr and t = 2050, then CO_2 projections for the year 2020, would be used to calculate DIC_{eq}^{t-age}; $DIC_{eq}^{2012-age}$ was calculated from equation (4). The ΔDIC_{anth} for subsurface waters was modeled for each projection year as a linear function of σ_θ, and the surface and subsurface ΔDIC_{anth} were connected assuming a two end member linear mixing between σ_θ 25.2 and 25.5 kg m^{-3} to prevent step changes (Figure 2).

2.4.2 Calculation of ΔDIC$_{bio}$

ΔDIC_{bio} was quantified following formulations in Sabine et al., 2002:

$$\Delta DIC_{bio} = r_{C:O}(AOU) - 0.5(TA_{obs} - TA^{\circ} + r_{N:O}(AOU)) \quad (6)$$

where *AOU* = Apparent Oxygen Utilization = ($O_{2,sat}$ – $O_{2,obs}$), *TA*° is the preformed alkalinity, and the *r*'s are the elemental remineralization ratios (Anderson and Sarmiento, 1994). The oxygen saturation concentration ($O_{2,sat}$) was calculated using the equations in *Garcia and Gordon*, 1992, and *TA*° was estimated based on historical near-surface *TA* data in the Pacific (equation 3 in Sabine et al., 2002). Phosphate concentrations necessary to estimate *TA*° were not directly measured, but were estimated from a regional empirical relationship using historical data

(Supplementary Materials); the uncertainty in estimating phosphate using this approach propagates to an error in $TA°$ of 4 µmol kg^{-1}.

2.4.3 Estimation of ΔDIC_{diseq}

Making accurate estimates of ΔDIC_{diseq} is important because it is a source of large uncertainty for anthropogenic carbon inventory calculations (Matsumoto and Gruber, 2005). Traditionally, age of the water mass is quantified using tracers such as CFCs and then the ΔDIC_{diseq} is subsequently calculated (Gruber et al., 1996; Sabine and Tanhua, 2010). However, such tracer measurements were not made for this study. Alternatively, we estimated ΔDIC_{diseq} based on θ & S data to overcome this limitation (Sabine et al., 2002). The mean θ and S between σ_θ of 25.5 and 26.5 kg m^{-3} were 10.0 °C and 33.9, respectively, resembling water type 1e in Sabine et al. (2010) with a corresponding ΔDIC_{diseq} = -6.24 µmol kg^{-1}, the value used in this study.

2.4.4 Calculation of the age of water parcel

In order to estimate the age of the water mass, we use equation (4) to calculate $DIC_{eq}^{2012-age}$, the DIC of the water parcel was in equilibrium with the atmosphere when it was last at the surface (i.e. equal to 2012 – age of the water mass). Therefore the age of the water mass can be calculated by comparing the atmospheric CO_2 record to the $pCO_{2,atm}$ that is necessary to generate $DIC_{eq}^{2012-age}$. The latter was calculated from the fugacity of CO_2 of the water mass when it was last in contact with the atmosphere at the time of subduction ($fCO_{2,eq}^{2012-age}$), assuming 100% relative humidity, and barometric pressure of 1 atm [Dickson, 2007]. The year that the water parcel subducted was determined by matching the calculated $CO_{2,atm}$ to the mean annual $CO_{2,atm}$ record (Keeling et al., 2005); the age is the difference

between 2012 and the calculated year (Figure 3). A relationship between σ_θ and the age was established by fitting a second order polynomial to the subsurface data (n = 186, R^2 = 0.92), and assuming the age of the surface water (σ_θ < 25.2) is 0 (Figure 3). The non-zero age of the water that appears around σ_θ = 24.4 kg m^{-3} corresponds to the shallow oxygen maximum layer that formed during the summer. However, since this density range is still shallower than the seasonal mixed layer, its age was considered to be 0. The age of the water ranged between 0 and 50 years between σ_θ of 25.2 and 26.5 kg m^{-3}.

2.4.5 Estimation of preindustrial DIC

In order to calculate the preindustrial DIC, equation (3) is written as:

$$DIC° = DIC_{\mathrm{eq}}^{\mathrm{prein}} + DIC_{\mathrm{anth}} + \Delta DIC_{\mathrm{diseq}} \quad (7)$$

where DIC_{anth} represents the anthropogenic carbon present in the water parcel in 2012, and $DIC_{\mathrm{eq}}^{\mathrm{prein}}$ is the DIC of the water parcel if it were in equilibrium with $pCO_{2,atm}$ = 280 µatm. Combining equations (2) and (7) and rearranging gives

$$DIC_{\mathrm{anth}} = DIC - \Delta DIC_{\mathrm{bio}} - DIC_{\mathrm{eq}}^{\mathrm{prein}} + \Delta DIC_{\mathrm{diseq}} \quad (8)$$

Calculated DIC_{anth} as a function of σ_θ is shown in Figure 4. Note that the values calculated here are in good agreement with published values using age tracers (Feely et al., 2008; Sabine et al., 2002) for higher σ_θ, but are significantly higher at lower densities. This is because the literature values were quantified using offshore subsurface waters, whereas our study region is near the coast along an upwelling margin, where subsurface waters are brought near the surface and are thus affected by surface processes. The agreement at higher density where surface influence is minimal demonstrates that the model presented here is capable of making accurate estimates of anthropogenic CO_2. Furthermore, the comparison illustrates the importance of incorporating surface influence when making acidification projections in shallow, coastal

ecosystems. Preindustrial DIC (DIC_{prein}) was calculated by subtracting DIC_{anth} from DIC observed in 2012. Preindustrial pCO_2, Ω_{Ar}, and pH were calculated using DIC_{prein} and TA conditions from 2012.

3 Results

3.1 Carbonate Chemistry Variability Observed in 2012

The results are presented using pH, pCO_2, or Ω_{Ar}, since pH was directly measured, and pCO_2 and Ω_{Ar} are commonly used as stress indicators for respiration (Brewer and Peltzer, 2009) and calcification (Langdon et al., 2010), respectively. Across all four sites in 2012, pCO_2 increased with depth. In 2012, the mean pCO_2 in the surf zone was near atmospheric equilibrium (394 µatm), while the mean pCO_2 at 88 m was 878 µatm (Table 2), and reached a maximum of 1270 µatm. The variability of pCO_2 also increased with depth (indicated by the s.d. of the time series), which was only 43 µatm in the surf zone, but was 149 µatm at 88-m depth. The mean (± 1 s.d.) Ω_{Ar} decreased with depth; the mean Ω_{Ar} in the surf zone was 2.4 ± 0.25, where it was 1.05 ± 0.18 at 88 m. Undersaturated conditions ($\Omega_{Ar} < 1$) were observed 48% of the time at 88 m in 2012, but were not observed at other sites. However, unlike pCO_2, the variability of Ω_{Ar}, indicated by the s.d., decreased with depth (0.25 at the surface to 0.18 at 88 m) (Table 2; see Discussion). The mean pH decreased with depth; the mean pH in the surfzone was 8.05, where it was 7.73 at 88 m. The variability in pH increased with depth until 30 m, but decreased at 88 m (Table 2).

Distinct, habitat-specific CO_2 signatures were observed at the four deployment sites (Figure 5, Figure 6, and Figure 7). Here, we define habitat-specific CO_2 signatures as how CO_2 conditions varied in that habitat, regardless of biological or physical origin. In the surf zone, the conditions were near atmospheric equilibrium, with intrusions of higher pCO_2 waters through

352 internal tidal bores, a common feature observed in shallow, upwelling environments (Booth et al.,
353 2012; Pineda, 1991); temperature and pH were correlated during these events (Supplementary
354 Figure 1). This leads to a high, mean daily range of CO_2 conditions (e.g. 96 µatm, 0.46, and
355 0.085 for pCO_2, Ω_{Ar}, and pH, respectively) (Table 3). However, the signature from the internal
356 bores usually only lasted several hours, and remained at near atmospheric equilibrium for the
357 large majority of the time. Higher occurrence of tidal bores were observed during the spring and
358 summer months relative to winter (Figure 5), consistent with previous observations (Pineda,
359 1991). The mean diel range of pCO_2 at the surf zone was significantly higher than measurements
360 made by a surface mooring located off shore in the SCB (Leinweber et al., 2009).

361 The mean (± s.d.) CO_2 conditions in the kelp forest and the canyon edge were similar,
362 and the s.d. for Ω_{Ar} and pH were the highest among the sites (Table 2). However, the timescales
363 of the variability were different, indicating that distinct processes control the CO_2 conditions in
364 these two habitats. For example, the mean daily range for all the variables was significantly
365 higher at the canyon edge compared to the kelp forest (Table 3). Submarine canyons are known
366 to amplify tidal energy (Navarro et al., 2013; Swart et al., 2011), and in fact, periodic variability
367 at the canyon edge occurred on semi-diurnal and diurnal cycles, indicative of tidal forcing.
368 Temeprature and pH were correlated on these shorter timescales (Supplementary Figure 1),
369 further supporting the fact that the variability was dominantly driven by intrusion of cold, deep
370 waters from the canyon.

371 While tidal forcings and daily biological production are drivers for carbonate chemistry
372 in the La Jolla kelp forest, the largest variability occurred on event time scales (Frieder et al.,
373 2012); event time scales are defined as longer than a day, but shorter than several weeks. For
374 example, pH, pCO_2, and Ω_{Ar} regularly changed by up to 0.3, 250 µatm, and 1.3 on event time

scales, more than three times the mean daily range. Variability on event time scales is due to a combination of changing water mass, stratification, and biological respiration (Frieder et al., 2012). In addition, a clear seasonal pattern was observed at the canyon edge, where higher pCO_2 and lower pH and Ω_{Ar} were observed during the spring and summer months (upwelling season) and lower pCO_2 and higher pH and Ω_{Ar} were observed during the fall and winter (relaxation season). Due to incomplete data coverage, a seasonal trend at the kelp forest and pier sites could not be discerned. The largest seasonal change among the four sites for Ω_{Ar} (~1) was observed at the canyon edge; pCO_2 differed by roughly 200–300 µatm between the two seasons.

The shelf break experienced the highest mean CO_2 conditions, and the highest and lowest s.d. for pCO_2 (149 µatm) and Ω_{Ar} (0.18), respectively (Table 2); the s.d. of pH (0.070) was lower than the kelp forest (0.083) or the canyon edge (0.075). Variability on tidal, event, and seasonal time scales were observed at this site (Figure 5, Figure 6, and Figure 7), as has been previously reported for oxygen (Send and Nam, 2012). In general, upwelling on event time scales led to greater changes in pCO_2 and pH than on tidal frequencies (Figure 5 and Figure 6). The largest variability for all parameters occurred between the seasons, where a change in pCO_2, pH, and Ω_{Ar} were approximately 350 µatm, 0.2, and 0.5, respectively. The close proximity of these four sites demonstrates the wide variety of habitat-specific CO_2 signatures that exist over a small spatial scale, especially in near shore environments.

3.2 Modeled Carbonate Chemistry

Each habitat showed distinct trends in both modeled mean and variability of pCO_2, pH, and Ω_{Ar} owing to increased levels of anthropogenic DIC (ΔDIC_{anth}) (Table 2). For example, the mean pCO_2 at the surf zone (4 m), canyon edge (30 m), and shelf break (88 m) increased by 225, 435, and 738 µatm, respectively, from 2012 to 2100; this drastic difference in increased mean

398 pCO_2 is driven by different buffer factors due to depth differences among the sites. The increase
399 in variability (i.e. s.d.) was also larger at 88 m (97 µatm) compared to the surf zone (37 µatm),
400 although the largest increase occurred at the canyon edge at 30 m (126 µatm) (Table 2). Similar
401 trends were observed for mean pH, where the largest mean decrease in pH occurred at 88-m
402 water depth (0.26). However, the s.d. increased into the future for the three shallowest sites,
403 whereas the s.d. decreased at the shelf break (88 m). In contrast, the largest decrease in the mean
404 Ω_{Ar} occurred at the surface relative to the deeper sites, whereas the decrease in range was
405 equivalent across all depths.

406 The measured and modeled time series for pCO_2 and Ω_{Ar} at the shelf break for the year
407 2012 and 2100 are shown in Figure 8 and Figure 9. The variability of pCO_2 increases on both
408 seasonal and tidal time scales; the seasonal amplitude increases from approximately 350 to 650
409 µatm and the mean daily range increases from 110 to 325 µatm by 2100. This greater variability
410 is in addition to an increase in mean pCO_2 of > 700 µatm. On the other hand, the variability of
411 Ω_{Ar} on both seasonal and shorter time scales decreases. Furthermore, the shelf break is projected
412 to experience undersaturated waters over 90% of the time by 2060, compared to 48% in 2012.
413 Similar patterns were observed in the kelp forest as well, where both the mean conditions and
414 variability of pCO_2 increased, and Ω_{Ar} decreased (Figure 10). The largest variability at the kelp
415 forest occurred on timescales of days to weeks, and high frequency (< 1 day) variability was
416 significantly smaller than at the shelf break. Therefore benthic organisms at the kelp forest would
417 experience elevated CO_2 conditions for prolonged periods of time, with only intermittent
418 exposure to near-atmospheric conditions.

419 Preindustrial pCO_2 and Ω_{Ar} were compared to conditions observed in 2012 (Table 2). At
420 most sites, the observed pCO_2, pH, and Ω_{Ar} in 2012 were already outside of their preindustrial

variability envelopes (defined as mean ± 1 s.d.), which is consistent with results from a previous ROMS simulation in the CCS (Hauri et al., 2013b). These results suggest that all habitats studied here have left, or are about to leave, the pCO_2, pH, and Ω_{Ar} conditions that were experienced during preindustrial times. This is significant as organisms at these sites are now surviving in conditions that are significantly different than the conditions under which their ancestors evolved.

The modeled habitat-specific pCO_2 and Ω_{Ar} conditions for preindustrial, 2012, 2060, and 2100 are shown in Figure 11. The histograms represent the full range of carbonate conditions at each habitat that was captured by the sensors, which includes both the seasonal and high-frequency variability. The shape of each distribution skews towards more "corrosive" conditions at all sites as the model steps forward into the future. This translates to not only increases in mean pCO_2, but also greater extremes and amount of time spent in extremes.

The projected pCO_2 and Ω_{Ar} envelopes (mean ± s.d.) at each habitat throughout the modeled period are shown in Figure 12. An increasing rate of change in pCO_2 (ΔpCO_2 yr^{-1}) is observed, whereas Ω_{Ar} tends to decrease at a relatively constant rate. The rate of increase of pCO_2 is higher than the projected atmospheric CO_2 increase at all subsurface sites. This indicates that as ocean acidification progresses, the effects due to elevated pCO_2 are more likely to become exacerbated with increasing depth. Mean Ω_{Ar} is projected to be < 1 at the shelf break by 2020, and leave the 2012 variability envelope around 2070.

4 Discussion

4.1 Changes in the Buffer Factors

The general patterns of the acidification trajectories presented here can be explained by changing buffer factors of seawater, as deeper sites are more strongly influenced by CO_2 rich upwelled waters. The buffer factors Π_{pCO2}, Π_{pH}, and Π_{CO3}, are defined as

$$\Pi_{pCO2} = \frac{\partial pCO_2}{\partial DIC}, \qquad \Pi_{pH} = \frac{\partial pH}{\partial DIC}, \qquad \Pi_{CO3} = \frac{\partial CO_3^{2-}}{\partial DIC} \tag{9}$$

representing the change in each carbonate parameter with respect to a change in DIC (Frankignoulle, 1994). The effect of temperature on Π is small (< 10%) between 0-15 °C for the DIC and TA values observed here, thus subsequent values were calculated assuming a temperature of 10 °C, TA = 2240 µmol kg^{-1}, and salinity = 33.5 (Figure 13). The ability for seawater to buffer changes in pCO_2 diminishes under higher concentrations of DIC. For example, Π_{pCO2} increases from 1.6 to 3.3 at the surface between 2012 and 2100 under the RCP6.0 scenario. However, since deeper waters are naturally elevated in DIC, this effect is more pronounced at the shelf break: Π_{pCO2} increases from 6.2 to 12.3 during the same time interval. This explains why the surf zone had the lowest mean increase in pCO_2 (225 µatm) despite having the highest increase in DIC (82 µmol kg^{-1}) out of all of the sites. The shelf break on the other hand had the highest increase in pCO_2 (737 µatm) while having the smallest increase in mean DIC (77 µmol kg^{-1}) during the same time period. Furthermore, the increase in variability with depth can be explained as well, as the same biological and physical forcings on tidal to seasonal cycles cause a larger change in pCO_2.

Changes in Π_{CO3} can explain the patterns for Ω_{Ar}, since $[Ca^{2+}]$ and K_{SP} remain unchanged. Unlike Π_{pCO2}, $|\Pi_{CO3}|$ decreases at higher concentrations of DIC (Figure 13B); $|\Pi_{CO3}|$ decreases from 0.62 to 0.57 at the surface, and 0.49 to 0.3 at 88 m between 2012 and 2100. This change in Π_{CO3} explains both the decrease in rate and range of Ω_{Ar} as anthropogenic CO_2 continues to infiltrate the ocean.

The Π_{pH} follows a parabolic shape, where there is a maximum decrease in pH per DIC added (Figure 13C). In a pure carbonate solution, this maximum occurs when DIC = TA, but in

seawater it occurs at slightly lower DIC (Frankignoulle, 1994); this maxima occurs at DIC = 2225 μmol kg^{-1} using the parameters listed above. Therefore we would expect to see a similar trend for pH as pCO_2, where greatest changes occur at depth relative to the surface as long as the mean DIC is lower than this threshold. This condition is only met at the shelf break (88 m) near the end of the century, thus as expected greater decrease in mean pH, and increase in variability (i.e. s.d.) was observed with depth (Table 2). One exception was observed where the s.d. decreased as ocean acidification progressed at the shelf break. This is because an increased proportion of time is spent at greater DIC where Π_{pH} is past its maxima, leading to a smaller variability in pH under the same changes in DIC. It is important to note that the buffer factor of H^+ (Π_{H+}) follows a similar pattern as pCO_2, where it continues to increase as DIC increases (Figure 13D). Therefore the rate of increase of $[H^+]$ will continue to increase as ocean acidification progresses, thus biological responses to $[H^+]$ may become exacerbated in the future.

4.2 Observed and Modeled Carbonate Chemistry Variability

The carbonate conditions presented here are consistent with previous studies. For example at the shelf break, Ω_{Ar} had a strong seasonal cycle, where undersaturated waters were observed almost continuously throughout the upwelling season (Nam et al., 2015), and remained supersaturated for the rest of the year. This is in good agreement with previous hydrographic surveys in this region, where aragonite-undersaturated waters have been observed as shallow as 60 m during the beginning of the upwelling season (Feely et al., 2008), but were not observed in the upper 100 m at the end of the upwelling season in this region (Bednaršek et al., 2014). Furthermore, estimates based on empirical equations showed a similar seasonal pattern in Ω_{Ar} at 88 m, where undersaturated waters were observed every upwelling season (Alin et al., 2012). However, undersaturated waters were not observed in the upper 30 m, unlike northern parts of

488 the CCS where undersaturated conditions are repeatedly observed at the surface during the
489 upwelling season (Bednaršek et al., 2014; Feely et al., 2008; Harris et al., 2013). Due to these
490 traits, the southern portion of the CCS is commonly considered less vulnerable to ocean
491 acidification compared to its northern counterpart. However, our results demonstrate that Ω_{Ar} as
492 low as 1.3 is routinely observed in the kelp forest (17 m), demonstrating the imminent threat of
493 anthropogenic ocean acidification to the southern CCS.

494 The subsurface habitats characterized in this study routinely experience Ω_{Ar} conditions
495 that have been shown to have non-lethal chronic effects on various bivalve larvae between Ω_{Ar} of
496 1.2 to 2.0 (Barton et al., 2012; Gaylord et al., 2011; Gazeau et al., 2011; Hettinger et al., 2012;
497 Waldbusser et al., 2015). However, the length of exposure to these unfavorable conditions varies
498 between habitats. For example, the organisms in the kelp forest would be exposed to low Ω_{Ar}
499 conditions for days to weeks, whereas large tidal variability at the canyon edge could result in
500 periodic exposure to low Ω_{Ar} conditions on the order of hours. Therefore the effects of low Ω_{Ar}
501 will largely depend on the reproductive timing and environmental variability that occurs on event
502 to seasonal time scales; the effects of exposure on various timescales are poorly understood.
503 Such events are expected to become more severe in the future (Hauri et al., 2013a), and thus
504 could lead to an increased rate of failed recruitment of bivalves and other keystone organisms
505 (Byrne et al., 2013).

506 It may be surprising that the mean diel range of pH was the smallest at the kelp forest
507 (Table 3), as one might expect a large diel cycle driven by photosynthesis and respiration in a
508 highly productive kelp forest. This is most likely because the sensor was deployed near the
509 benthos, below the most productive region of the forest. Frieder et al. 2012 observed
510 significantly larger diel pH variability closer to the surface (7 m depth) compared to near the

511 bottom (17 m depth; same as this study), demonstrating that the biologically driven diel cycle
512 diminishes with increasing depth within the canopy. Therefore it is important to keep in mind
513 that the results presented here are not reflecting kelp forest production dynamics, rather, reflect
514 conditions that are experienced by benthic dwelling organisms inside the kelp forest.

515 The trajectories are sensitive to the choice of the emission scenario (Figure 14). Trends
516 are similar at all depths, thus only the mean pCO_2 and Ω_{Ar} projections at the shelf break are
517 shown in Figure 14. The highest emission scenario (RCP8.5) diverges from the two intermediate
518 scenarios around 2030, while the lowest emission scenario (RCP2.6) diverges around 2050. The
519 two intermediate scenarios (RCP4.5 and RCP6.0) do not diverge significantly until 2070. The
520 delayed response to different atmospheric CO_2 trajectories occurs because upwelled waters have
521 spent several decades since they were last in contact with the atmosphere (Feely et al., 2008).
522 Therefore the anthropogenic ocean acidification trajectory for the Southern California Bight is
523 already determined for the next several decades, and any mitigation due to changing CO_2
524 emissions will be delayed.

525 The results presented here are site specific, and do not necessarily reflect conditions at all
526 kelp forests, canyon edges, and shelf breaks. However, if sensor pH data and corresponding
527 regional hydrographic surveys are available, then a ΔDIC_{anth}–σ_θ relationship can be established
528 for that region and applied to the sensor data. For example, this approach can potentially
529 expanded to many regions for the CCS, using the North American Carbon Program West Coast
530 Cruise (Feely et al., 2008) and the ΔDIC_{diseq} for the Pacific Ocean (Sabine et al., 2002). If similar
531 data exist, then this approach can be expanded to other upwelling margins as well.

532 The Southern California Bight experiences a steady but weaker degree of upwelling
533 compared to the northern regions of the CCS, where upwelling events are more pronounced

(Bograd et al., 2009). These regions could experience more extreme conditions regularly, as well as significantly higher variability of carbonate conditions (Harris et al., 2013). However, such dynamics are poorly understood, and more high-frequency observations of carbonate parameters along this system are needed. Source water properties must be characterized through hydrographic surveys. Alternatively, for regions where such data for source waters are not available, sensor data can be combined with either Global Circulation Model or ROMS outputs. This approach will alleviate the cost associated with characterizing source waters, and to a large degree will incorporate processes such as interannual variability, decadal changes in source water properties, and reduced ventilation. It is critical that inorganic carbon sensors (e.g. pH or pCO_2) are co-located with basic physical oceanographic measurements (e.g. T and S) to determine source water properties especially for subsurface deployments.

4.3 Model Assessment

The sensitivity of the projected carbonate conditions to the assumptions made in the model is explored here. For example, temperatures observed in 2012 were used to parameterize the model. Sea surface temperature has increased over the past century due to climate change (Smith et al., 2008), and is expected to continue. This will affect the CO_2 equilibrium concentration (DIC_{eq}), but the effects are small and will reduce DIC_{eq} by only several μmol kg^{-1}. Both pCO_2 and Ω_{Ar} are dependent on in situ temperature; the effects on Ω_{Ar} are negligible ($\Delta\Omega/\Delta T < 0.01°C^{-1}$), whereas $\Delta pCO_2/\Delta T$ increases at higher pCO_2 levels, and can be as large as 60 μatm $°C^{-1}$ at the end of the century, compared to 30 μatm $°C^{-1}$ at present day at the shelf break. These temperature dependencies will affect the mean conditions, but the magnitude of the variability will be relatively unaffected. However, it should be noted that this simple error analysis does not include any biological feedbacks that increased temperature or CO_2 may induce.

For example, phase shifts from kelp-dominated to algal turfs might be an outcome of sea surface warming and acidification (Connell and Russell, 2010), with implications for habitat-scale biogeochemical cycling. Likewise, higher temperatures may increase remineralization rates along the path of the subducted water (Rivkin and Legendre, 2001), further enhancing acidification.

TA conditions from 2012 were used to calculate pCO_2 and Ω_{Ar} for all years. Changes in TA affect the buffer factors of seawater, thus, alterations in TA distribution will either speed up or slow down the progression of ocean acidification. However, trends in TA along the CCS on decadal time scales are unknown due to insufficient data. Reduced ventilation in high latitude seas, altered precipitation patterns, and changes in surface calcification and water-column dissolution rates would all lead to changes in upwelled TA conditions (Fassbender et al., 2011; Lee et al., 2006). Quantifying these processes is difficult and out of the scope of this study. Nevertheless, to demonstrate the magnitude of the uncertainty due to TA, pCO_2 was projected for the year 2100 with a +20 µmol kg^{-1} bias to TA. The effects were strongly dependent on depth: mean pCO_2 was reduced by approximately 240, 130, and 70 µatm at 88 m, 30 m, and the surface, respectively.

Finally, the model presented here projects future carbonate conditions by assuming the dynamics that control the variability at each habitat (e.g. seasonal and episodic upwelling events, internal waves and tides, and biological production and respiration) remain the same as 2012 conditions, and does not account for any variability that occurs on inter-annual to decadal timescales. For example, changes in O_2 and pH on the continental shelf associated with interannual climate events, such as El Niño, have been observed (Nam et al., 2011). However, since 2012 did not correspond with a strong El Niño or La Niña phase, we believe that it was not

strongly biased by such events. Furthermore, recent evidence suggests that the proportion of Pacific Equatorial Waters in the California Undercurrent has been increasing over the past several decades, thus modifying the source water properties for upwelled waters onto the continental shelf (Bograd et al., 2015). Since waters of equatorial origin observed between 100-500 m are elevated in DIC and lower in O_2 (Bograd et al., 2015), it is expected that the Southern California Bight will experience higher levels of acidification than predicted from this study if this redistribution of water masses of equatorial origin continues. However, at this time, we lack observations with sufficient longevity to predict how climate variability on interannual to decadal time scales might modify the acidification trajectory over the course of the next century. Sustained, high-frequency time series of inorganic carbon parameters are required to elucidate such effects.

4.4 Implications for Ocean Acidification Research

In order to properly assess the impacts of anthropogenic ocean acidification through laboratory manipulation experiments, the control and experimental conditions should accurately reflect the study organism's present-day and future habitat conditions (McElhany and Busch, 2013; Reum et al., 2015). The most common control treatment used in ocean acidification experiments for organisms found in the CCS was a pCO_2 value of ~400 µatm, reflecting atmospheric conditions (compiled by Reum et al., 2015). However, our sensor data showed that all subsurface habitats had significantly greater pCO_2 relative to the atmosphere (Table 2). For example, the mean pCO_2 at the kelp forest is about 100 µatm greater than the atmosphere, and routinely experiences conditions of more than 300 µatm above atmospheric. Therefore utilizing atmospheric pCO_2 conditions for control treatments will necessarily underestimate the baseline pCO_2 for organisms collected from subsurface habitats.

603 Recent studies that incorporate natural variability into ocean acidification experiments
604 observed modified responses relative to constant conditions (Dufault et al., 2012; Frieder et al.,
605 2014). However, the effect of natural variability on organismal response to ocean acidification,
606 especially through various life stages is still poorly understood. Our model results demonstrate
607 that variability trajectories are also habitat specific. For example, in the kelp forest, the
608 variability, approximated by the s.d., was 93 µatm in 2012, whereas this increased to 202 µatm
609 in 2100 (Table 2). Furthermore, despite having similar mean CO_2 conditions, the largest
610 variability was observed on event time scales in the kelp forest, whereas the dominant variability
611 occurred on tidal and seasonal cycles at the canyon edge. Therefore future ocean acidification
612 studies investigating the effect of natural variability should not only incorporate increasing
613 magnitude into their experimental design, but also consider variability patterns on appropriate
614 time scales.

615 Temperature and O_2 were tightly correlated with carbonate parameters across habitats
616 and various time scales (daily to seasonal) in this study (Figure 15); similar correlation has been
617 documented across the CCS in general (Reum et al., 2014, 2015). These parameters can
618 potentially act as additional stressors (Padilla-Gamiño et al., 2013) or stress reliefs (Gooding et
619 al., 2009) for ocean acidification. However, laboratory experiments incorporating the effects of
620 temperature (Gooding et al., 2009; Padilla-Gamiño et al., 2013) and O_2 (Frieder et al., 2014;
621 Navarro et al. *in prep*) have just started to be explored for the CCS, and no studies have been
622 conducted that incorporate all three variables in their experimental design. Future studies
623 investigating the synergistic effects of O_2, temperature, and CO_2 should establish experimental
624 conditions based on environmental data (Figure 15). Although development of systems that can
625 manipulate individual parameters is challenging, important strides have been made to make such

626 experimental set ups accessible to the community (Bockmon et al., 2013). The development of
627 habitat-specific ocean acidification models provides a link between environment and laboratory
628 to facilitate interpretations of physiological responses to elevated CO_2 in the context of current
629 and future environmental conditions.

630 Discerning habitat-specific CO_2 signatures could lead to the discovery of local
631 populations that are more tolerant of future CO_2 conditions. For example, large high-frequency
632 variability of CO_2 could lead to a greater capacity for physiological and phenotypic plasticity, as
633 organisms are routinely exposed to a wide range of CO_2. The embryos of Doryteuthis opalescens,
634 an important fishery species in California, can tolerate low pH and O_2, perhaps due to the fact
635 that they routinely experience a wide range of pH and O_2 (Navarro, 2014). Furthermore, such
636 environmental conditions may be conducive for the existence of high CO_2 tolerant
637 subpopulations, allowing for adaptation to buffer some of the negative effects of ocean
638 acidification (Hofmann and Todgham, 2010). Alternatively, these populations could be living
639 near critical biological thresholds, as has been suggested for the thermal stress of some
640 organisms living in the intertidal (Somero, 2002). A massive failure in an oyster hatchery in
641 Oregon was linked to upwelling of high CO_2 waters during a critical life-stage of oyster larvae
642 (Barton et al., 2012), indicating the existence of CO_2 thresholds for some marine organisms
643 (Bednaršek et al., 2014). However, such thresholds may be dependent on species, life-stage,
644 and/or environmental history. As we begin to realize which populations of species and life stages
645 are living near acidification thresholds versus those that exhibit acidification tolerance,
646 implementation of habitat-specific acidification models can be used as a tool to aid protection,
647 management and remediation efforts of critical marine habitats now and in the future.

5 Conclusions

Here we have presented habitat-specific carbonate chemistry projections for four coastal habitats along an upwelling margin. The projections were generated by combining high-frequency sensor measurements, a regional empirical relationship for TA, hydrographic survey data to quantify source-water properties of upwelled waters, and the atmospheric CO_2 record. Even though the four habitats were within 5 km of one another, distinct habitat-specific variability signatures and acidification trajectories were observed. These results reveal the existence of highly variable CO_2 signatures within a small geographic area, and the potential for discoveries of habitats that could act as refugia from ocean acidification. Changes in the buffer factors largely explained the observed patterns; however, local biological feedbacks could also produce a large acidification signal. In all habitats studied, carbonate conditions have left, or are leaving preindustrial variability envelopes. Model projections suggest that anthropogenic ocean acidification will continue to progress in the CCS and other upwelling margins over the next several decades regardless of any changes in CO_2 emissions; any impacts from reduced emissions will only be observed mid-century and beyond. This demonstrates the urgency of the situation, and this delayed response must be taken into account when assessing the impacts of ocean acidification and developing mitigation and monitoring strategies.

6 Acknowledgements

Hydrographic data and kelp forest time series data are available at BCO-DMO project SeapHOx (http://www.bco-dmo.org/project/2122). Sensor time series data are available for the Del Mar buoy at http://mooring.ucsd.edu, and upon request for the Scripps Pier (smithj@ucsd.edu).

We would like to thank the University of California Ship Funds for providing ship time for maintenance of the Del Mar Buoy and the San Diego Coastal Expedition cruises. We thank Emily Kelly for DIC analysis at sea, and all of the ship crew and volunteers that aided in sample collection. We would like to thank Emily Donham for providing discrete TA data from the kelp forest. The Del Mar Buoy platform has been maintained by the Ocean Time-series Group (http://mooring.ucsd.edu); we acknowledge their efforts to continuously collect and maintain the time-series data. The canyon edge deployment was supported by the NOAA Grant #NA10OAR4170060 and the California Sea Grant College Program Project #R/CC-04. The kelp forest deployment was supported by NSF-OCE Award No. 0927445. We would also like to thank the Ellen Browning Scripps Foundation, the Scripps Family Foundation, the Bohn and Grand families, and the California State Water Board for financial support for the Scripps Ocean Acidification Real-time Monitoring Program. S. Nam was partly supported by the Research Resettlement Fund for the new faculty of Seoul National University and Korean Ministry of Oceans and Fisheries through EAST-I program. Financial support for Richard A. Feely was provided by the National Oceanic and Atmospheric Administration under the NOAA Ocean Acidification Program and the Climate Observations Division of the NOAA Climate Program, Contribution Number 4313 from the NOAA Pacific Marine Environmental Laboratory. The statements, findings, conclusions and recommendations are those of the authors and do not necessarily reflect the views of California Sea Grant, state agencies, NOAA, NSF or the U.S. Department of Commerce.

Literature Cited

Alin, S. R., Feely, R. A., Dickson, A. G., Hernández-Ayón, J. M., Juranek, L. W., Ohman, M. D. and Goericke, R.: Robust empirical relationships for estimating the carbonate system in the southern California Current System and application to CalCOFI hydrographic cruise data (2005–2011), J. Geophys. Res., 117(C5), C05033, doi:10.1029/2011JC007511, 2012.

Anderson, L. A. and Sarmiento, J. L.: Redfield ratios of remineralization determined by nutrient data analysis, Global Biogeochem. Cycles, 8(1), 65–80, 1994.

Andersson, A. J., Yeakel, K. L., Bates, N. R. and de Putron, S. J.: Partial offsets in ocean acidification from changing coral reef biogeochemistry, Nat. Clim. Chang., 3(11), 1–6, doi:10.1038/nclimate2050, 2013.

Barton, A., Hales, B., Waldbusser, G. G., Langdon, C. and Feely, R. A.: The Pacific oyster, Crassostrea gigas, shows negative correlation to naturally elevated carbon dioxide levels: Implications for near-term ocean acidification effects, Limnol. Oceanogr., 57(3), 698–710, doi:10.4319/lo.2012.57.3.0698, 2012.

Bates, N. R., Astor, Y. M., Church, M. J., Currie, K., Dore, J. E., Gonzalez-Davila, M., Lorenzoni, L., Muller-Karger, F., Olafsson, J. and Santana-Casiano, J. M.: A time-series view of changing surface ocean chemistry due to ocean uptake of anthropogenic CO2 and ocean acidification, Oceanography, 27(1), 126–141, 2014.

Bednaršek, N., Feely, R. A., Reum, J. C. P., Peterson, B., Menkel, J., Alin, S. R. and Hales, B.: Limacina helicina shell dissolution as an indicator of declining habitat suitability owing to ocean acidification in the California Current Ecosystem., Proc. R. Soc. B Biol. Sci., 281(1785), 20140123, doi:10.1098/rspb.2014.0123, 2014.

Bockmon, E. E., Frieder, C. A., Navarro, M. O., White-Kershek, L. A. and Dickson, A. G.: Technical note: controlled experimental aquarium system for multi-stressor investigation of carbonate chemistry, oxygen saturation, and temperature, Biogeosciences, 10(9), 5967–5975, doi:10.5194/bg-10-5967-2013, 2013.

Bograd, S. J., Buil, M. P., Lorenzo, E. Di, Castro, C. G., Schroeder, I. D., Goericke, R., Anderson, C. R., Benitez-Nelson, C. and Whitney, F. A.: Changes in source waters to the Southern California Bight, Deep Sea Res. Part II Top. Stud. Oceanogr., 112, 42–52, doi:10.1016/j.dsr2.2014.04.009, 2015.

Bograd, S. J., Schroeder, I., Sarkar, N., Qiu, X., Sydeman, W. J. and Schwing, F. B.: Phenology of coastal upwelling in the California Current, Geophys. Res. Lett., 36(1), 1–5, doi:10.1029/2008GL035933, 2009.

Booth, J. A. T., McPhee-Shaw, E. E., Chua, P., Kingsley, E., Denny, M., Phillips, R., Bograd, S. J., Zeidberg, L. D. and Gilly, W. F.: Natural intrusions of hypoxic, low pH water into nearshore

marine environments on the California coast, Cont. Shelf Res., 45, 108–115, doi:10.1016/j.csr.2012.06.009, 2012.

Bresnahan, P. J., Martz, T. R., Takeshita, Y., Johnson, K. S. and LaShomb, M.: Best practices for autonomous measurement of seawater pH with the Honeywell Durafet, Methods Oceanogr., 9, 44–60, 2014.

Brewer, P. G. and Peltzer, E. T.: Limits to marine life, Science (80-.)., 324(5925), 347–348, 2009.

Byrne, M., Lamare, M., Winter, D., Dworjanyn, S. A. and Uthicke, S.: The stunting effect of a high CO2 ocean on calcification and development in sea urchin larvae, a synthesis from the tropics to the poles, Philos. Trans. R. Soc. B Biol. Sci., 368(1627), 1–13, doi:10.1098/rstb.2012.0439, 2013.

Byrne, R. H., Mecking, S., Feely, R. A. and Liu, X.: Direct observations of basin-wide acidification of the North Pacific Ocean, Geophys. Res. Lett., 37(2), 1–5, doi:10.1029/2009GL040999, 2010.

Cai, W.-J., Hu, X., Huang, W.-J., Murrell, M. C., Lehrter, J. C., Lohrenz, S. E., Chou, W.-C., Zhai, W., Hollibaugh, J. T., Wang, Y., Zhao, P., Guo, X., Gundersen, K., Dai, M. and Gong, G.-C.: Acidification of subsurface coastal waters enhanced by eutrophication, Nat. Geosci., 4(11), 766–770, doi:10.1038/ngeo1297, 2011.

Carter, B. R., Radich, J. A., Doyle, H. L. and Dickson, A. G.: An automated system for spectrophotometric seawater pH measurements, Limnol. Oceanogr. Methods, 11, 16–27, doi:10.4319/lom.2013.11.16, 2013.

Clayton, T. D. and Byrne, R. H.: Spectrophotometric seawater pH measurements: total hydrogen ion concentration scale calibration of m-cresol purple and at-sea results, Deep Sea Res. Part I Oceanogr. Res. Pap., 40(10), 2115–2129, 1993.

Connell, S. D. and Russell, B. D.: The direct effects of increasing CO2 and temperature on non-calcifying organisms: increasing the potential for phase shifts in kelp forests., Proc. Biol. Sci., 277(1686), 1409–1415, doi:10.1098/rspb.2009.2069, 2010.

Dickson, A. G., Sabine, C. L. and Christian, J. R., Eds.: Guide to best practices for ocean CO2 measurements, PICES Special Publication 3., 2007.

Duarte, C. M., Hendriks, I. E., Moore, T. S., Olsen, Y. S., Steckbauer, A., Ramajo, L., Carstensen, J., Trotter, J. A. and McCulloch, M.: Is ocean acidification an open-ocean syndrome? Understanding anthropogenic impacts on seawater pH, Estuaries and Coasts, 36(2), 221–236, doi:10.1007/s12237-013-9594-3, 2013.

759 Dufault, A. M., Cumbo, V. R., Fan, T.-Y. and Edmunds, P. J.: Effects of diurnally oscillating
760 pCO2 on the calcification and survival of coral recruits, Proc. R. Soc. B Biol. Sci., 279(1740),
761 2951–2958, doi:10.1098/rspb.2011.2545, 2012.

762 Emerson, S. R.: Accurate measurement of O2, N2, and Ar gases in water and the solubility of N2,
763 Mar. Chem., 64(4), 337–347, doi:10.1016/S0304-4203(98)00090-5, 1999.

764 Fassbender, A. J., Sabine, C. L., Feely, R. A., Langdon, C. and Mordy, C. W.: Inorganic carbon
765 dynamics during northern California coastal upwelling, Cont. Shelf Res., 31(11), 1180–1192,
766 doi:10.1016/j.csr.2011.04.006, 2011.

767 Feely, R. A., Alin, S. R., Newton, J., Sabine, C. L., Warner, M., Devol, A., Krembs, C. and
768 Maloy, C.: The combined effects of ocean acidification, mixing, and respiration on pH and
769 carbonate saturation in an urbanized estuary, Estuar. Coast. Shelf Sci., 88(4), 442–449,
770 doi:10.1016/j.ecss.2010.05.004, 2010.

771 Feely, R. A., Doney, S. C. and Cooley, S. R.: Ocean acidification: present conditions and future
772 changes in a high-CO2 world, Oceanography, 22(4), 36–47, 2009.

773 Feely, R. A., Sabine, C. L., Hernandez-Ayon, J. M., Ianson, D. and Hales, B.: Evidence for
774 upwelling of corrosive "acidified" water onto the continental shelf., Science, 320(5882), 1490–
775 1492, doi:10.1126/science.1155676, 2008.

776 Frankignoulle, M.: A complete set of buffer factors for acid/base CO2 system in seawater, J. Mar.
777 Syst., 5(2), 111–118, 1994.

778 Frieder, C. A., Gonzalez, J. P., Bockmon, E. E., Navarro, M. O. and Levin, L. A.: Can variable
779 pH and low oxygen moderate ocean acidification outcomes for mussel larvae?, Glob. Chang.
780 Biol., 20(3), 754–64, doi:10.1111/gcb.12485, 2014.

781 Frieder, C. A., Nam, S., Martz, T. R. and Levin, L. A.: High temporal and spatial variability of
782 dissolved oxygen and pH in a nearshore California kelp forest, Biogeosciences, 9(10), 3917–
783 3930, doi:10.5194/bg-9-3917-2012, 2012.

784 Friederich, G. E., Walz, P. M., Burczynski, M. G. and Chavez, F. P.: Inorganic carbon in the
785 central California upwelling system during the 1997 – 1999 El Niño–La Niña event, Prog.
786 Oceanogr., 54(1-4), 185–203, 2002.

787 Garcia, H. E. and Gordon, L. I.: Oxygen solubility in seawater: better fitting equations, Limnol.
788 Oceanogr., 37(6), 1307–1312, 1992.

789 Gaylord, B., Hill, T. M., Sanford, E., Lenz, E. A., Jacobs, L. A., Sato, K. N., Russell, A. D. and
790 Hettinger, A.: Functional impacts of ocean acidification in an ecologically critical foundation
791 species, J. Exp. Biol., 214(Pt 15), 2586–2594, 2011.

792 Gazeau, F., Gattuso, J.-P., Greaves, M., Elderfield, H., Peene, J., Heip, C. H. R. and Middelburg,
793 J. J.: Effect of carbonate chemistry alteration on the early embryonic development of the Pacific
794 oyster (Crassostrea gigas), PLoS One, 6(8), e23010, doi:10.1371/journal.pone.0023010, 2011.

795 Gooding, R. A., Harley, C. D. G. and Tang, E.: Elevated water temperature and carbon dioxide
796 concentration increase the growth of a keystone echinoderm, Proc. Natl. Acad. Sci. U. S. A.,
797 106(23), 9316–9321, doi:10.1073/pnas.0811143106, 2009.

798 Gruber, N., Hauri, C., Lachkar, Z., Loher, D., Frölicher, T. L. and Plattner, G.-K.: Rapid
799 progression of ocean acidification in the California Current System, Science (80-.)., 337(6091),
800 220–223, doi:10.1126/science.1216773, 2012.

801 Gruber, N., Lachkar, Z., Frenzel, H., Marchesiello, P., Münnich, M., McWilliams, J. C., Nagai, T.
802 and Plattner, G.-K.: Eddy-induced reduction of biological production in eastern boundary
803 upwelling systems, Nat. Geosci., 4(11), 787–792, doi:10.1038/ngeo1273, 2011.

804 Gruber, N., Sarmiento, J. L. and Stocker, T. F.: An improved method for detecting anthropogenic
805 CO2 in the oceans, Global Biogeochem. Cycles, 10(4), 809–837, 1996.

806 Hales, B., Takahashi, T. and Bandstra, L.: Atmospheric CO2 uptake by a coastal upwelling
807 system, Global Biogeochem. Cycles, 19(1), 1–11, doi:10.1029/2004GB002295, 2005.

808 Hall-Spencer, J. M., Rodolfo-Metalpa, R., Martin, S., Ransome, E., Fine, M., Turner, S. M.,
809 Rowley, S. J., Tedesco, D. and Buia, M.-C.: Volcanic carbon dioxide vents show ecosystem
810 effects of ocean acidification, Nature, 454(7200), 96–99, 2008.

811 Harris, K. E., DeGrandpre, M. D. and Hales, B.: Aragonite saturation state dynamics in a coastal
812 upwelling zone, Geophys. Res. Lett., 40(11), 2720–2725, doi:10.1002/grl.50460, 2013.

813 Hauri, C., Gruber, N., McDonnell, A. M. P. and Vogt, M.: The intensity, duration, and severity
814 of low aragonite saturation state events on the California continental shelf, Geophys. Res. Lett.,
815 40(13), 3424–3428, doi:10.1002/grl.50618, 2013a.

816 Hauri, C., Gruber, N., Vogt, M., Doney, S. C., Feely, R. A., Lachkar, Z., Leinweber, A.,
817 McDonnel, A. M. P., Munnich, M. and Plattner, G.-K.: Spatiotemporal variability and long-term
818 trends of ocean acidification in the California Current System, Biogeosciences, 10(1), 193–216,
819 2013b.

820 Hettinger, A., Sanford, E., Hill, T. M., Russell, A. D., Sato, K. N. S., Hoey, J., Forsch, M., Page,
821 H. N. and Gaylord, B.: Persistent carry-over effects of planktonic exposure to ocean acidification
822 in the Olympia oyster, Ecology, 93(12), 2758–2768, doi:10.1890/12-0567.1, 2012.

823 Van Heuven, S., Pierrot, D., Rae, J. W. B., Lewis, E. and Wallace, D. W. .: MATLAB Program
824 Developed for CO2 System Calculations. ORNL/CDIAC-105b., ,
825 doi:10.3334/CDIAC/otg.CO2SYS_MATLAB_v1.1, 2011.

826 Hijioka, Y., Matsuoka, Y., Nishimoto, H., Masui, M. and Kainuma, M.: Global GHG emissions
827 scenarios under GHG concentration stabilization targets, J. Glob. Environ. Eng., 13, 97–108,
828 2008.

829 Hofmann, G. E., Evans, T. G., Kelly, M. W., Padilla-Gamiño, J. L., Blanchette, C. A., Washburn,
830 L., Chan, F., McManus, M. A., Menge, B. A., Gaylord, B., Hill, T. M., Sanford, E., LaVigne, M.,
831 Rose, J. M., Kapsenberg, L. and Dutton, J. M.: Exploring local adaptation and the ocean
832 acidification seascape – studies in the California Current Large Marine Ecosystem,
833 Biogeosciences, 11(4), 1053–1064, doi:10.5194/bg-11-1053-2014, 2014.

834 Hofmann, G. E., Smith, J. E., Johnson, K. S., Send, U., Levin, L. A., Micheli, F., Paytan, A.,
835 Price, N. N., Peterson, B., Takeshita, Y., Matson, P. G., Crook, E. D., Kroeker, K. J., Gambi, M.
836 C., Rivest, E. B., Frieder, C. A., Yu, P. C. and Martz, T. R.: High-frequency dynamics of ocean
837 pH: a multi-ecosystem comparison, edited by W.-C. Chin, PLoS One, 6(12), e28983,
838 doi:10.1371/journal.pone.0028983, 2011.

839 Hofmann, G. E. and Todgham, A. E.: Living in the now: physiological mechanisms to tolerate a
840 rapidly changing environment., Annu. Rev. Physiol., 72, 127–45, doi:10.1146/annurev-physiol-
841 021909-135900, 2010.

842 Keeling, C. D., Piper, S. C., Bacastow, R. B., Wahlen, M., Whorf, T. P., Heimann, M. and
843 Meijer, H. A.: Atmospheric CO2 and 13CO2 exchange with the terrestrial biosphere and oceans
844 from 1978 to 2000: observations and carbon cycle implications, in A history of atmospheric CO2
845 and its effects on plants, animals, and ecosystems, edited by J. R. Ehleringer, T. E. Cerling, and
846 M. D. Dearing, pp. 83–113, Springer Verlag, New York., 2005.

847 Kroeker, K. J., Micheli, F., Gambi, M. C. and Martz, T. R.: Divergent ecosystem responses
848 within a benthic marine community to ocean acidification, Proc. Natl. Acad. Sci. U. S. A.,
849 108(35), 14515–14520, doi:10.1073/pnas.1107789108, 2011.

850 Langdon, C., Gattuso, J. and Andersson, A.: Measurements of calcification and dissolution of
851 benthic organisms and communities, in Guide to Best Practices for Ocean Acidificaton Research
852 and Data Reporting, pp. 213–232, Publications Office of the European Union, Luxembourg.,
853 2010.

854 Lauvset, S. K. and Gruber, N.: Long-term trends in surface ocean pH in the North Atlantic, Mar.
855 Chem., 162, 71–76, doi:10.1016/j.marchem.2014.03.009, 2014.

856 Lee, K., Tong, L. T., Millero, F. J., Sabine, C. L., Dickson, A. G., Goyet, C., Park, G.-H.,
857 Wanninkhof, R., Feely, R. A. and Key, R. M.: Global relationships of total alkalinity with
858 salinity and temperature in surface waters of the world's oceans, Geophys. Res. Lett., 33(19), 1–
859 5, doi:10.1029/2006GL027207, 2006.

860 Leinweber, A. and Gruber, N.: Variability and trends of ocean acidification in the Southern
861 California Current System: a time series from Santa Monica Bay, J. Geophys. Res. Ocean.,
862 118(7), 3622–3633, doi:10.1002/jgrc.20259, 2013.

Leinweber, A., Gruber, N., Frenzel, H., Friederich, G. E. and Chavez, F. P.: Diurnal carbon cycling in the surface ocean and lower atmosphere of Santa Monica Bay, California, Geophys. Res. Lett., 36(8), 3–7, doi:10.1029/2008GL037018, 2009.

Liu, X., Patsavas, M. C. and Byrne, R. H.: Purification and characterization of meta-cresol purple for spectrophotometric seawater pH measurements, Environ. Sci. Technol., 45(11), 4862–4868, doi:10.1021/es200665d, 2011.

Lueker, T. J., Dickson, A. G. and Keeling, C. D.: Ocean pCO2 calculated from dissolved inorganic carbon, alkalinity, and equations for K1 and K2: validation based on laboratory measurements of CO2 in gas and seawater at equilibrium, Mar. Chem., 70(1-3), 105–119, doi:10.1016/S0304-4203(00)00022-0, 2000.

Martz, T. R., Connery, J. G. and Johnson, K. S.: Testing the Honeywell Durafet for seawater pH applications, Limnol. Oceanogr. Methods, 8, 172–184, doi:10.4319/lom.2010.8.172, 2010.

Martz, T. R., Send, U., Ohman, M. D., Takeshita, Y., Bresnahan, P., Kim, H.-J. and Nam, S.: Dynamic variability of biogeochemical ratios in the Southern California Current System, Geophys. Res. Lett., 41(7), 2496–2501, doi:10.1002/2014GL059332, 2014.

Martz, T. R., Takeshita, Y., Rolph, R. and Bresnahan, P.: Tracer monitored titrations: measurement of dissolved oxygen., Anal. Chem., 84(1), 290–296, doi:10.1021/ac202537f, 2012.

Matsumoto, K. and Gruber, N.: How accurate is the estimation of anthropogenic carbon in the ocean? An evaluation of the ΔC* method, Global Biogeochem. Cycles, 19(3), 1–17, doi:10.1029/2004GB002397, 2005.

McElhany, P. and Busch, D. S.: Appropriate pCO2 treatments in ocean acidification experiments, Mar. Biol., 160(8), 1807–1812, doi:10.1007/s00227-012-2052-0, 2013.

McNeil, B. I. and Matear, R. J.: Southern Ocean acidification: a tipping point at 450-ppm atmospheric CO2, Proc. Natl. Acad. Sci. U. S. A., 105(48), 18860–18864, doi:10.1073/pnas.0806318105, 2008.

Mehrbach, C., Culberson, C. H., Hawley, J. E. and Pytkowicz, R. M.: Measurement of the apparent dissociation constants of carbonic acid in seawater at atmospheric pressure, Limnol. Oceanogr., 18(6), 897–907, doi:10.4319/lo.1973.18.6.0897, 1973.

Nam, S., Kim, H.-J. and Send, U.: Amplification of hypoxic and acidic events by La Niña conditions on the continental shelf off California, Geophys. Res. Lett., 38(22), 1–5, doi:10.1029/2011GL049549, 2011.

Nam, S., Takeshita, Y., Frieder, C. A., Martz, T. and Ballard, J.: Seasonal advection of Pacific Equatorial Water alters oxygen and pH in the Southern California Bight, J. Geophys. Res. Ocean., 120, n/a–n/a, doi:10.1002/2015JC010859, 2015.

Navarro, M. O.: Consequences of environmental variability for spawning and embryo development of inshore market squid Doryteuthis opalescens, Ph.D. thesis, Unviersity of California San Diego. Ann Arbor, USA, ProQuest Dissertations and Theses (Publication No. 3644287)., 2014.

Navarro, M. O., Parnell, P. E. and Levin, L. A.: Year-round spawning of the Market Squid, Doryteuthis opalescens and associated critical habitat along an upwelling margin, in Coastal and Estuarine Research Federation National Conference, San Diego., 2013.

O'Sullivan, D. W. and Millero, F. J.: Continual measurement of the total inorganic carbon in surface seawater, Mar. Chem., 60(1-2), 75–83, doi:10.1016/S0304-4203(97)00079-0, 1998.

Padilla-Gamiño, J. L., Kelly, M. W., Evans, T. G. and Hofmann, G. E.: Temperature and CO2 additively regulate physiology, morphology and genomic responses of larval sea urchins, Strongylocentrotus purpuratus, Proc. R. Soc. B Biol. Sci., 280(1759), 20130155, doi:10.1098/rspb.2013.0155, 2013.

Pineda, J.: Predictable upwelling and the shoreward transport of planktonic larvae by internal tidal bores, Science (80-.)., 253(5019), 548–551, 1991.

Price, N. N., Martz, T. R., Brainard, R. E. and Smith, J. E.: Diel variability in seawater pH relates to calcification and benthic community structure on coral reefs, PLoS One, 7(8), e43843, doi:10.1371/journal.pone.0043843, 2012.

Reum, J. C. P., Alin, S. R., Feely, R. A., Newton, J., Warner, M. and McElhany, P.: Seasonal carbonate chemistry covariation with temperature, oxygen, and salinity in a fjord estuary: Implications for the design of ocean acidification experiments, PLoS One, 9(2), e89619, doi:10.1371/journal.pone.0089619, 2014.

Reum, J. C. P., Alin, S. R., Harvey, C. J., Bednarsek, N., Evans, W., Feely, R. A., Hales, B., Lucey, N., Mathis, J. T., McElhany, P., Newton, J., Newton, J. and Sabine, C. L.: Interpretation and design of ocean acidification experiments in upwelling systems in the context of carbonate chemistry co-variation with temperature and oxygen, ICES J. Mar. Sci., 528–536, doi:10.1093/icesjms/fsu231, 2015.

Rivkin, R. B. and Legendre, L.: Biogenic carbon cycling in the upper ocean: effects of microbial respiration., Science, 291(5512), 2398–2400, doi:10.1126/science.291.5512.2398, 2001.

Rodolfo-Metalpa, R., Houlbrèque, F., Tambutté, É., Boisson, F., Baggini, C., Patti, F. P., Jeffree, R., Fine, M., Foggo, a., Gattuso, J.-P. and Hall-Spencer, J. M.: Coral and mollusc resistance to ocean acidification adversely affected by warming, Nat. Clim. Chang., 1(6), 308–312, doi:10.1038/nclimate1200, 2011.

Rykaczewski, R. R. and Dunne, J. P.: Enhanced nutrient supply to the California Current Ecosystem with global warming and increased stratification in an earth system model, Geophys. Res. Lett., 37(21), 1–5, doi:10.1029/2010GL045019, 2010.

933 Sabine, C. L., Feely, R. A., Key, R. M., Bullister, J. L., Millero, F. J., Lee, K., Peng, T.-H.,
934 Tilbrook, B., Ono, T. and Wong, C. S.: Distribution of anthropogenic CO2 in the Pacific Ocean,
935 Global Biogeochem. Cycles, 16(4), 1–17, doi:10.1029/2001GB001639, 2002.

936 Sabine, C. L. and Tanhua, T.: Estimation of anthropogenic CO2 inventories in the ocean, Ann.
937 Rev. Mar. Sci., 2(1), 175–198, doi:10.1146/annurev-marine-120308-080947, 2010.

938 Send, U. and Nam, S.: Relaxation from upwelling: the effect on dissolved oxygen on the
939 continental shelf, J. Geophys. Res., 117(4), 1–9, doi:10.1029/2011JC007517, 2012.

940 Smith, T. M., Reynolds, R. W., Peterson, T. C. and Lawrimore, J.: Improvements to NOAA's
941 historical merged land–ocean surface temperature analysis (1880–2006), J. Clim., 21(10), 2283–
942 2296, doi:10.1175/2007JCLI2100.1, 2008.

943 Somero, G. N.: Thermal physiology and vertical zonation of intertidal animals: optima, limits,
944 and costs of living, Integr. Comp. Biol., 42(4), 780–789, 2002.

945 Sunda, W. G. and Cai, W.-J.: Eutrophication induced CO2-acidification of subsurface coastal
946 waters: interactive effects of temperature, salinity, and atmospheric pCO2, Environ. Sci.
947 Technol., 46(19), 10651–10659, doi:10.1021/es300626f, 2012.

948 Sutton, A. J., Feely, R. A., Sabine, C. L., McPhaden, M. J., Takahashi, T., Chavez, F. P.,
949 Friederich, G. E. and Mathis, J. T.: Natural variability and anthropogenic change in equatorial
950 Pacific surface ocean pCO2 and pH, Global Biogeochem. Cycles, 28(2), 1–15,
951 doi:10.1002/2013GB004679, 2014.

952 Swart, N. C., Allen, S. E. and Greenan, B. J. W.: Resonant amplification of subinertial tides in a
953 submarine canyon, J. Geophys. Res., 116(9), 1–14, doi:10.1029/2011JC006990, 2011.

954 Waldbusser, G. G., Hales, B., Langdon, C. J., Haley, B. A., Schrader, P., Brunner, E. L., Gray, M.
955 W., Miller, C. A. and Gimenez, I.: Saturation-state sensitivity of marine bivalve larvae to ocean
956 acidification, Nat. Clim. Chang., 5, 273–280, doi:10.1038/NCLIMATE2479, 2015.

957

Table 1: Summary of sensor deployments

Habitat Type	Deployment Site	DD[a]	BD[b]	Latitude	Longitude	Days[c]
Surf Zone	Scripps Pier	4	6	32.87°N	117.26°W	122
Kelp Forest	La Jolla Kelp Forest	17	20	32.81°N	117.29°W	128
Canyon Edge[d]	La Jolla Canyon	30	30	32.86°N	117.27°W	302
Shelf Break	Del Mar Buoy	88	100	32.94°N	117.32°W	335

[a] Sensor deployment depth in meters

[b] Bottom depth in meters

[c] Total deployment days between June 2012 and June 2013.

[d] A linear drift correction for salinity was applied for 2 of the 4 deployments.

964 Table 2. Mean ± s.d of modeled carbonate parameters at in situ conditions for preindustrial, 2012,
965 2060, and 2100 using the RCP6.0 projection at each habitat.

	Year	pCO_2 (µatm)	Ω_{Ar}	pH
Surf Zone	Preind.	267 ± 26	3.09 ± 0.21	8.19 ± 0.034
(4m)	2012	394 ± 43	2.38 ± 0.25	8.05 ± 0.038
	2060	473 ± 56	2.09 ± 0.19	7.98 ± 0.041
	2100	619 ± 80	1.71 ± 0.18	7.88 ± 0.045
Kelp Forest	Preind.	365 ± 74	2.28 ± 0.42	8.08 ± 0.078
(17 m)	2012	516 ± 108	1.77 ± 0.36	7.95 ± 0.083
	2060	683 ± 156	1.43 ± 0.33	7.84 ± 0.094
	2100	937 ± 231	1.11 ± 0.29	7.72 ± 0.105
Canyon Edge	Preind.	365 ± 68	2.29 ± 0.37	8.08 ± 0.068
(30 m)	2012	529 ± 105	1.75 ± 0.31	7.94 ± 0.075
	2060	702 ± 155	1.40 ± 0.29	7.83 ± 0.085
	2100	964 ± 231	1.09 ± 0.25	7.70 ± 0.095
Shelf Break	Preind.	637 ± 132	1.38 ± 0.27	7.86 ± 0.083
(88 m)	2012	878 ± 149	1.05 ± 0.18	7.73 ± 0.070
	2060	1195 ± 200	0.80 ± 0.15	7.61 ± 0.070
	2100	1639 ± 246	0.60 ± 0.10	7.47 ± 0.065

966

967

968 Table 3. Mean daily range of carbonate parameters at in situ conditions for 2012 at each habitat.

	pCO_2 (µatm)	**Ω_{Ar}**	**pH**
Surf Zone	96	0.46	0.085
Kelp Forest	68	0.22	0.054
Canyon Edge	167	0.48	0.120
Shelf Break	110	0.14	0.053

969

970

971

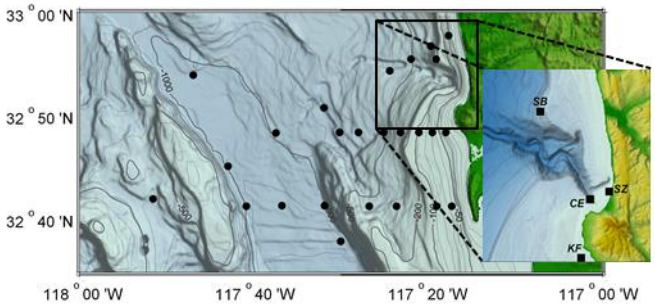

972

973 Figure 1: Map of study region. Hydrographic stations (black dots) and sensor deployment sites
974 (black squares) are shown. Initials are: CE = canyon edge, SB = shelf break, SZ = surf zone, and
975 KF = kelp forest.
976

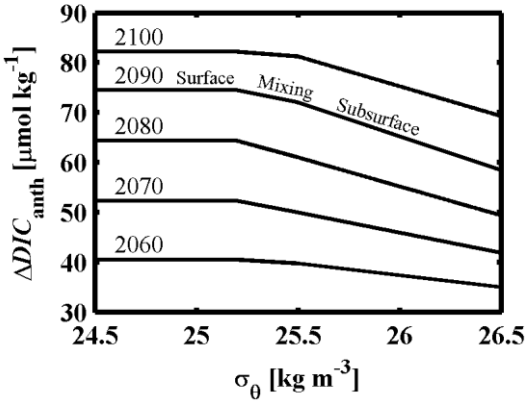

977

978 Figure 2: ΔDIC_{anth} as a function of σ_θ for certain modeled years (indicated above line) using the
979 ICPP RCP6.0 projection. The three regimes used in this model, surface, mixing, and subsurface,
980 are labeled.
981

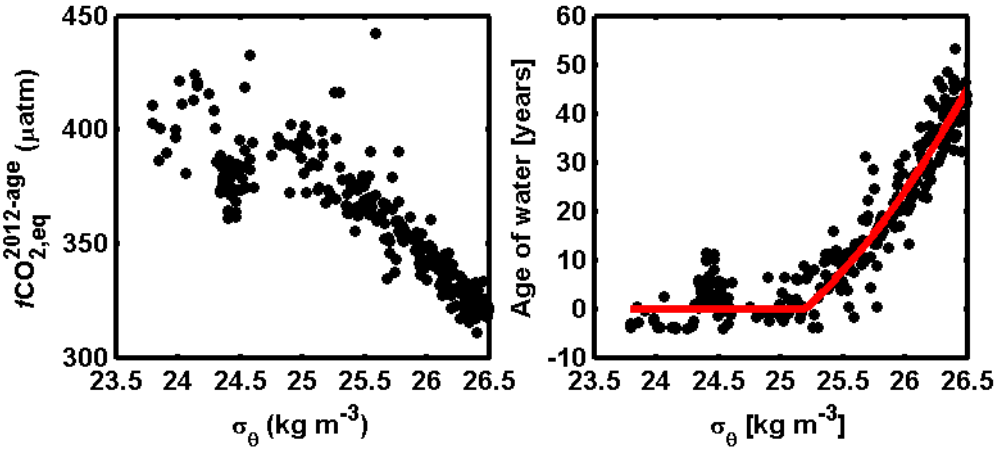

982

983 Figure 3: $fCO_{2,eq}^{2012-age}$ calculated from hydrographic data (left) and the calculated age-σθ
984 relationship (right) is shown. Good agreement (R2 = 0.87) between the data (black circles) and
985 the fit (age = 8.852(σθ – 25.2)2 + 23.132(σθ – 25.2); red line) is observed (right). Age of surface
986 waters (σ_θ < 25.2 kg m^{-3}) was assumed to be 0.
987

988

989

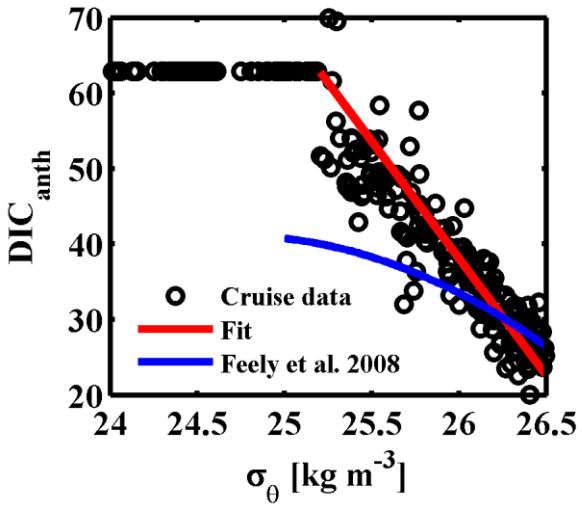

990
991 Figure 4: DIC_{anth} as a function of σ_θ. The calculated values and the fit are represented by black
992 circles and a red line, respectively. The blue line shows DIC_{anth} using the formulations from
993 Feely et al. (2008).
994

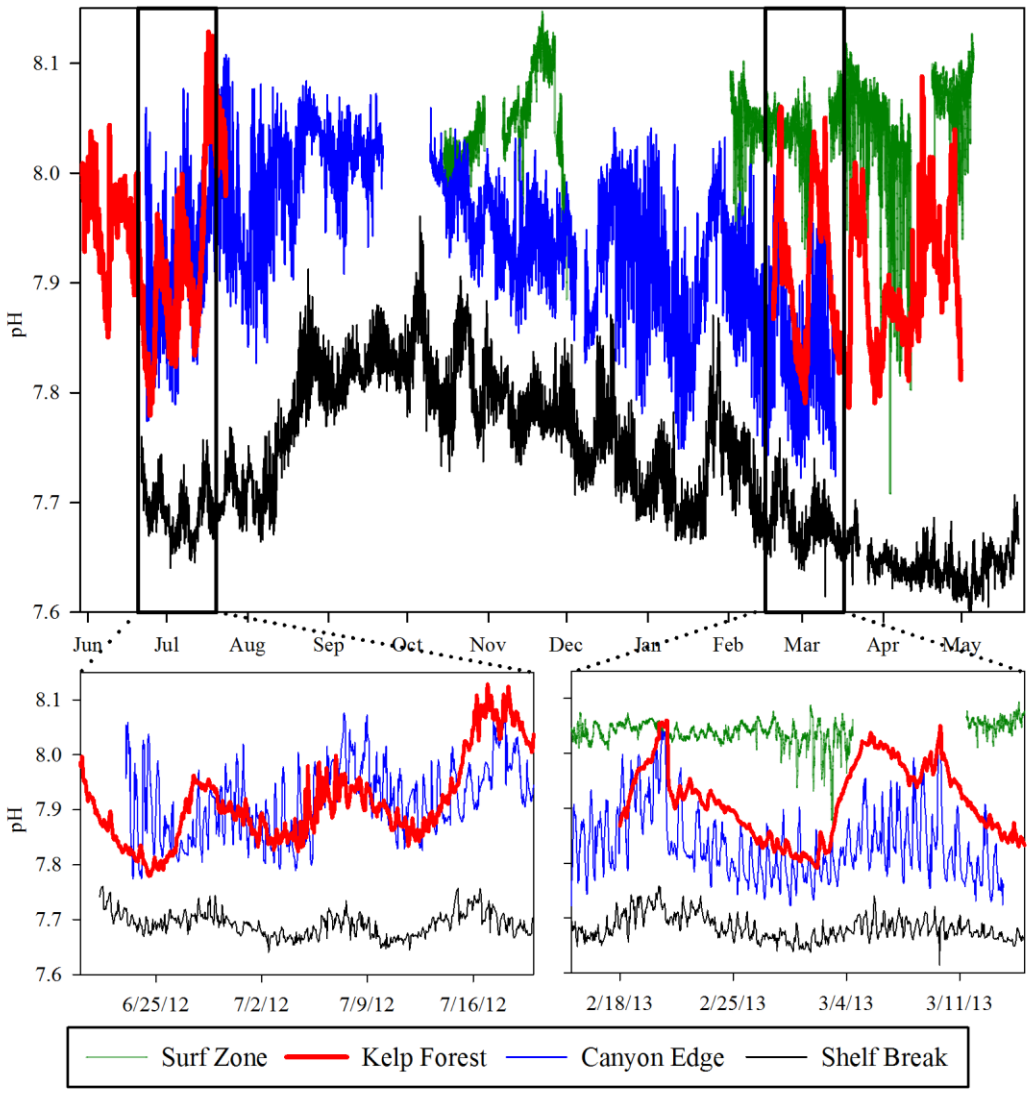

995

996 Figure 5: Time series of sensor pH between June 2012 to June. Two lower panels are month-long
997 snapshots. pH is reported at in situ conditions.
998

999

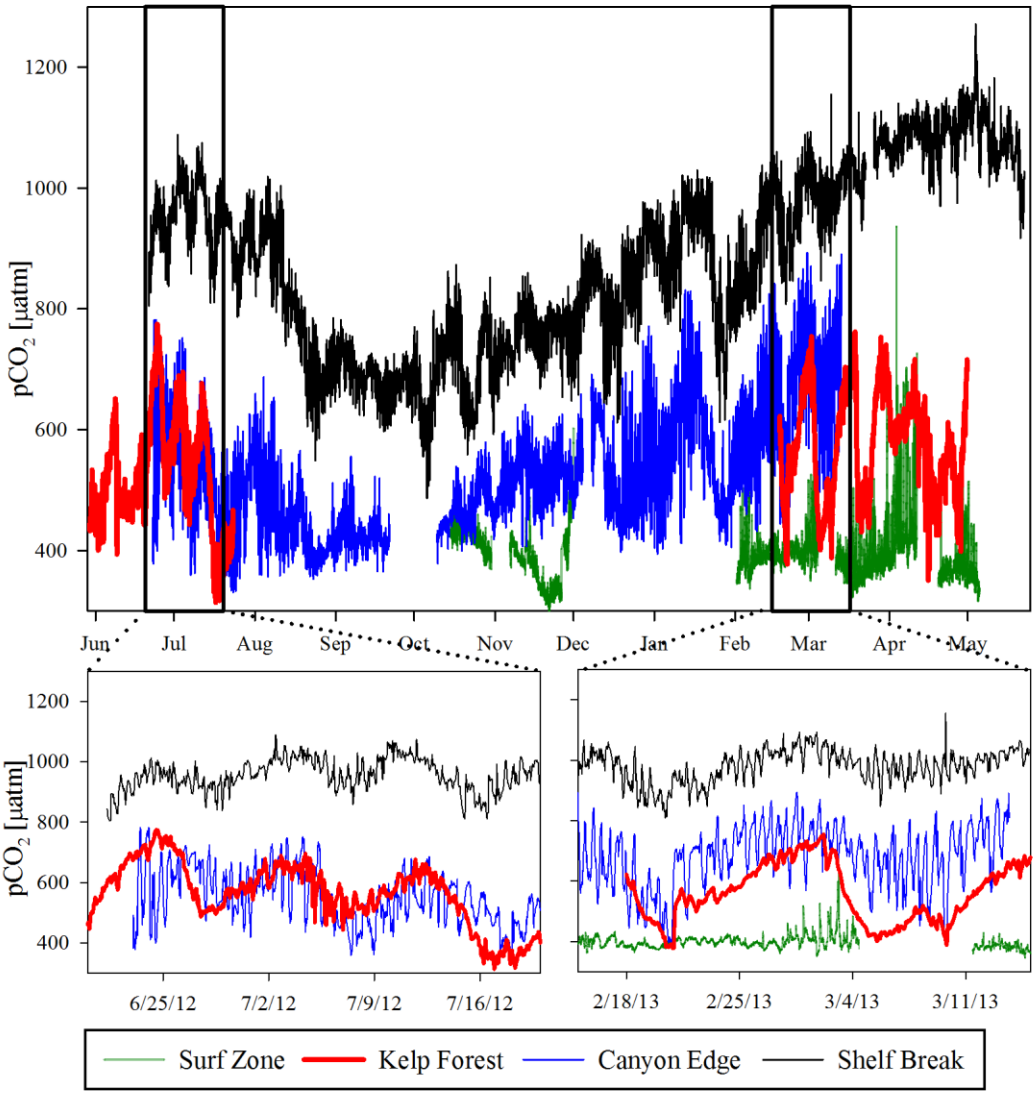

1000

1001 Figure 6: Time series of pCO_2 calculated from sensor pH and TA^{est} between June 2012 to June
1002 2013. Two lower panels are month-long snapshots. pCO_2 is reported at in situ conditions.
1003

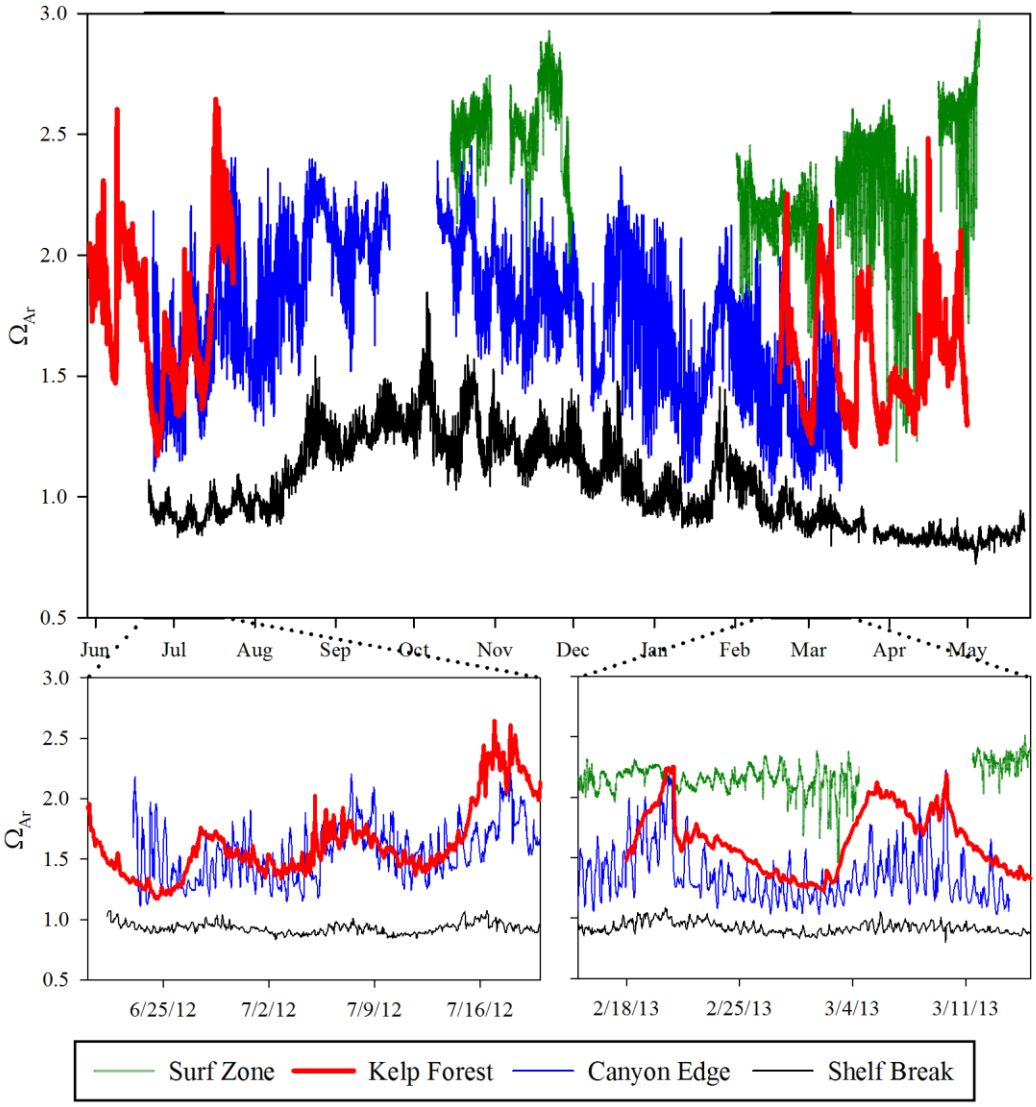

Figure 7: Time series of Ω_{Ar} calculated from sensor pH and TA^{est} between June 2012 to June 2013. Two lower panels are month-long snapshots. Ω_{Ar} is reported at in situ conditions.

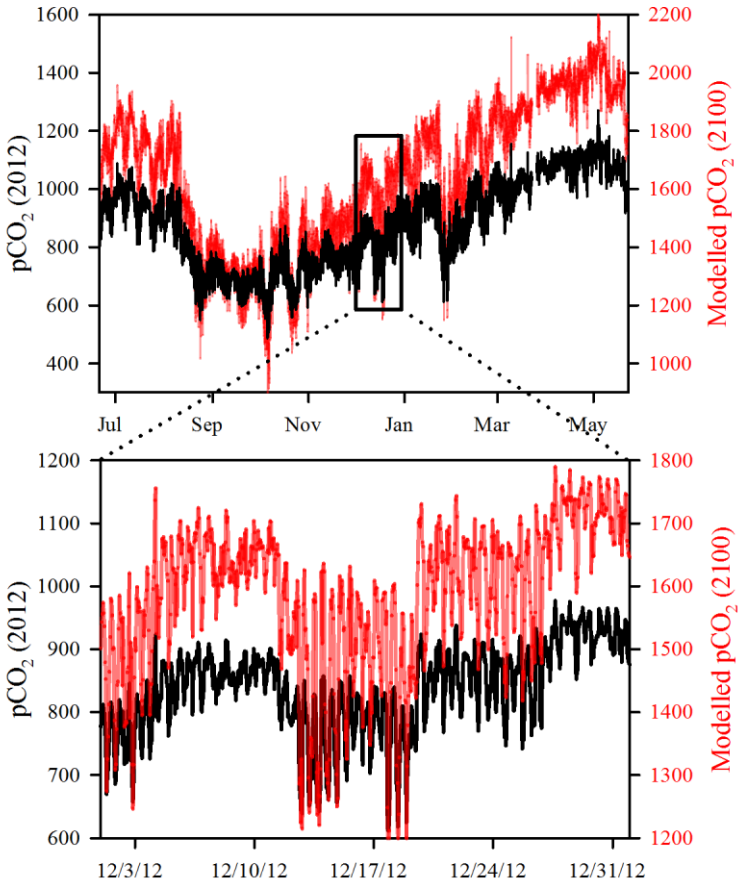

Figure 8: Observed pCO_2 in 2012 (black) and modeled pCO_2 using the IPCC RCP 6.0 scenario for the year 2100 (red) at the Del Mar Buoy (88 m) over an annual cycle (top). A close up for the month of December is shown on the bottom. Note that the range, but not the absolute values, of the vertical axes for each figure is the same.

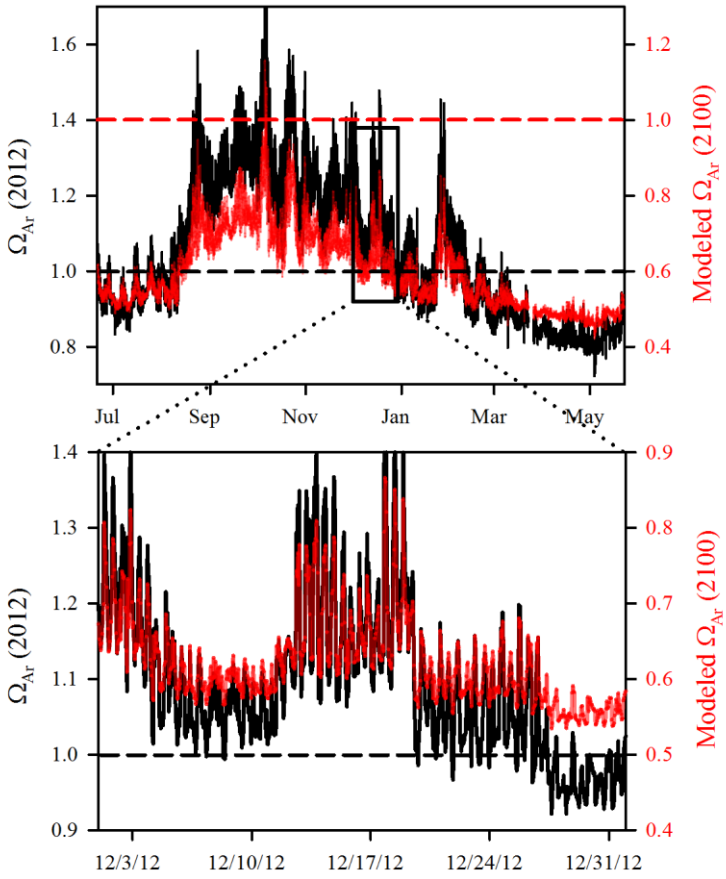

Figure 9: Observed Ω_{Ar} in 2012 (black) and modeled Ω_{Ar} using the IPCC RCP6.0 scenario for the year 2100 (red) at the shelf break (88 m) over an annual cycle (top). A close up for the month of December is shown on the bottom. Dashed lines represent Ω_{Ar} = 1. Note that the range, but not the absolute values, of the vertical axes for each figure is the same.

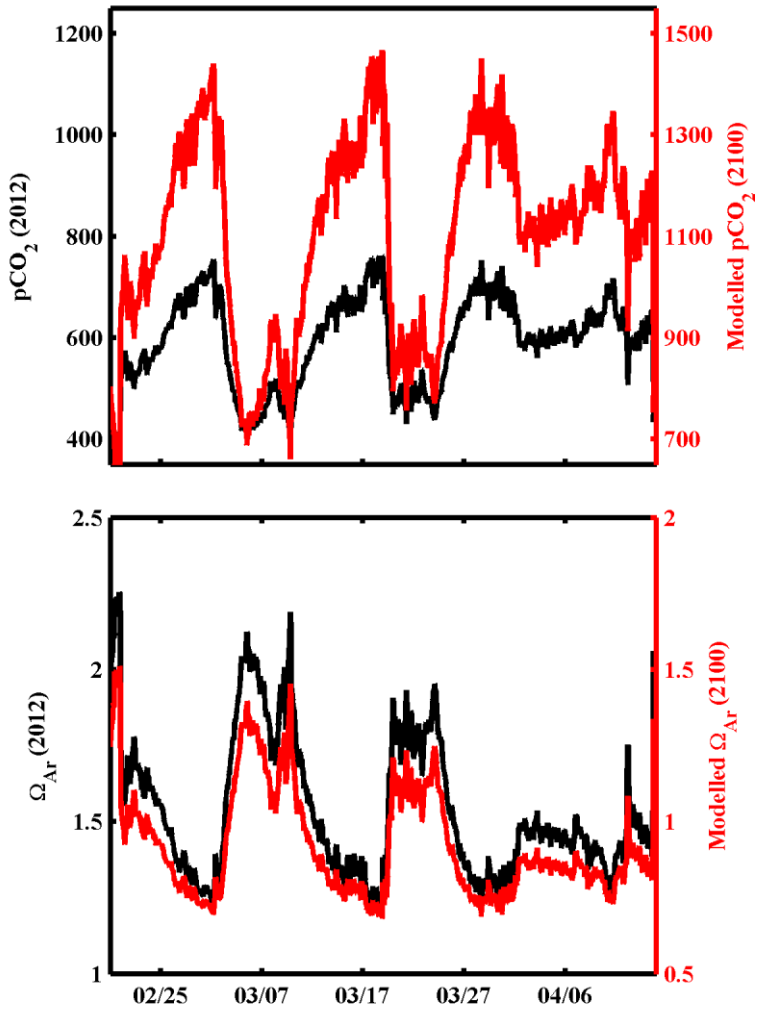

Figure 10: Observed (black) and modelled (red) pCO_2 (top) and Ω_{Ar} (bottom) at the La Jolla kelp forest (17 m). Modelled values correspond to projected values in 2100 using the IPCC RCP6.0 scenario. Note that the range, but not the absolute values, of the vertical axes for each figure is the same.

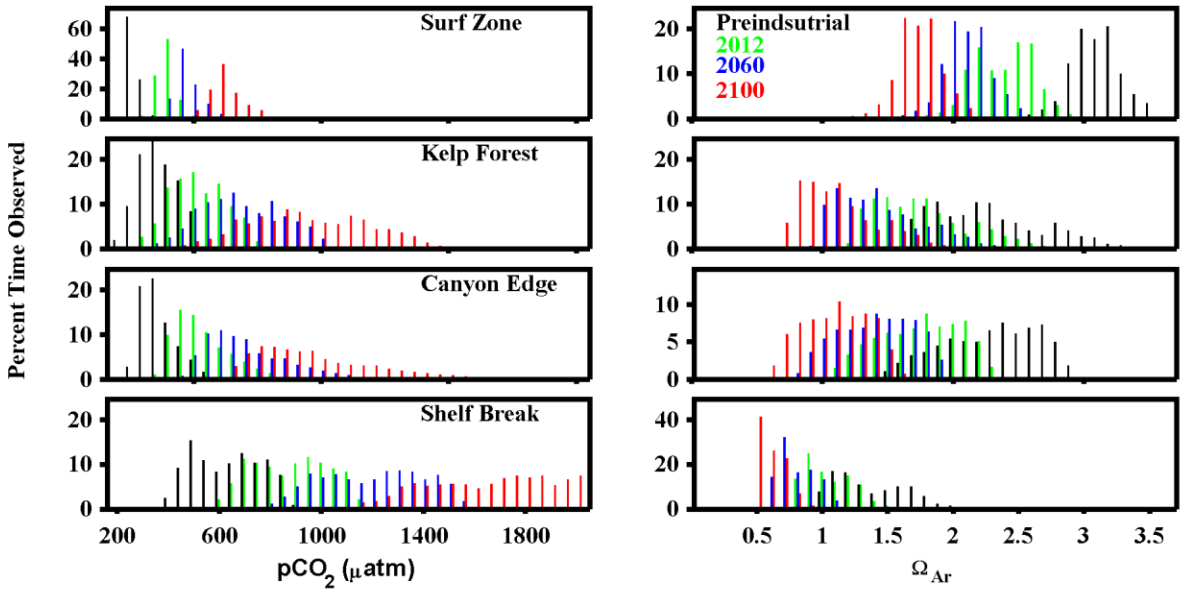

Figure 11: Histogram of modeled pCO_2 (left) and Ω_{Ar} (right) distribution at the four depths for preindustrial (black), 2012 (green), 2060 (blue), and 2100 (red). Atmospheric pCO_2 for the years 2060 and 2100 roughly correspond to 510 and 670 µatm based on the IPCC RCP6.0 scenario.

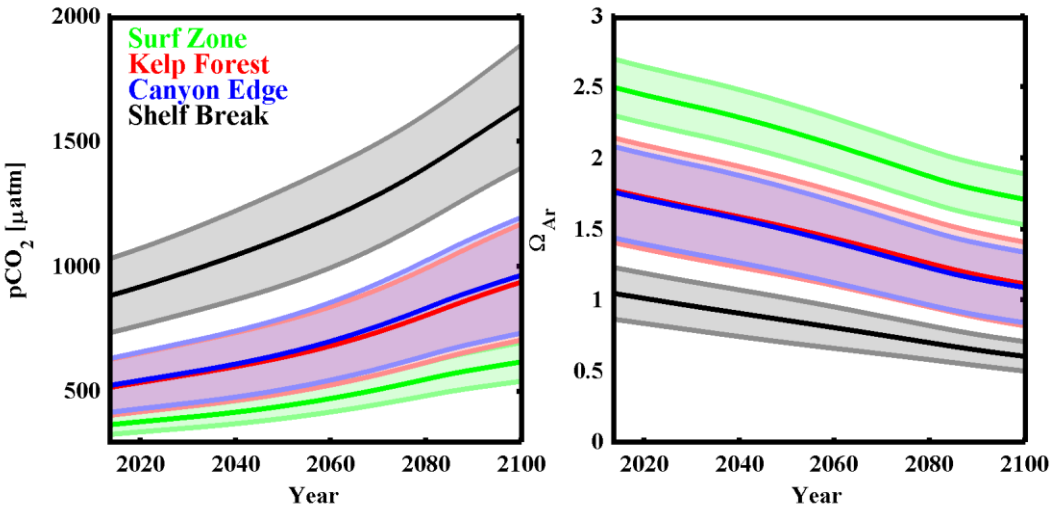

Figure 12: Projected pCO_2 (left) and Ω_{Ar} (right) between 2013 and 2100 under the IPCC RCP6.0 scenario. The solid line and the shaded region represent the mean and ± 1 s.d., respectively.

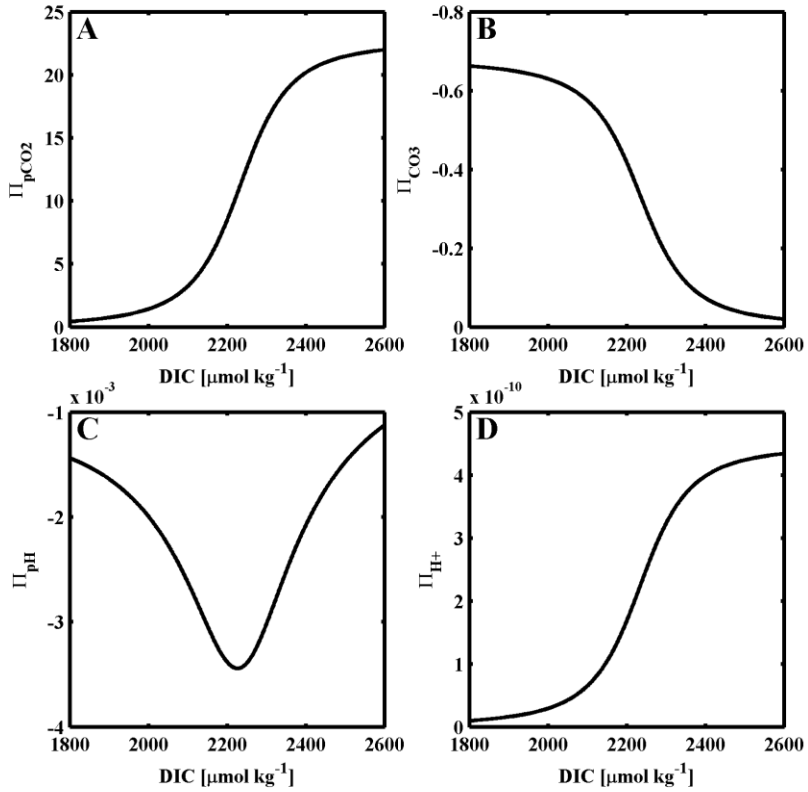

1035

1036 Figure 13: Buffer factor Π for pCO_2 (A), CO_3^{2-} (B), pH (C), and $[H^+]$ (D) as a function of DIC.
1037 Note the inverted y axis in panels B and C. Model parameters to calculate the Π values were: TA
1038 = 2240 µmol kg^{-1}, temperature = 10 °C, salinity = 33.5, pressure = 1.013 bar.
1039

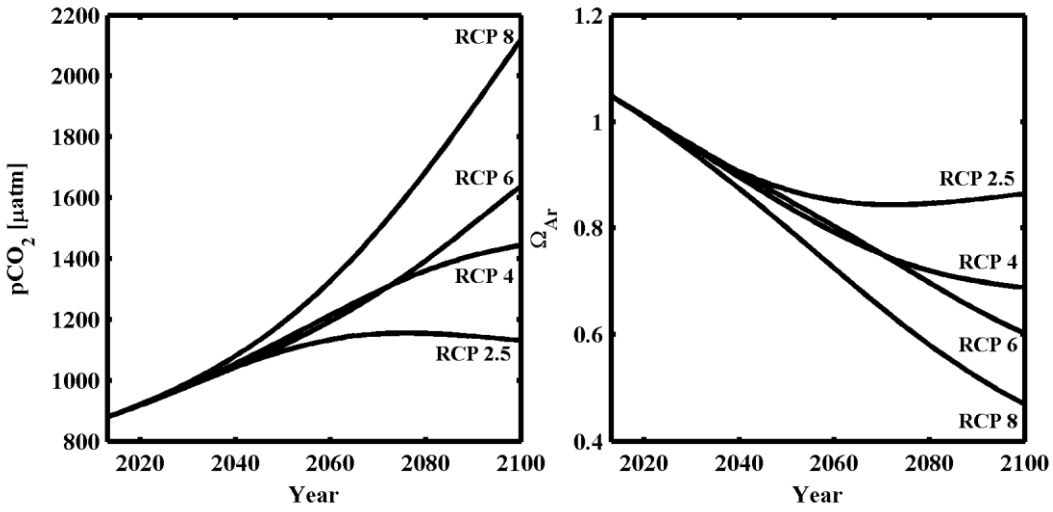

1040

1041 Figure 14: Projections of mean pCO_2 (left) and Ω_{Ar} (right) at the shelf break (88 m) based on
1042 four projections from the Fifth Assessment of the IPCC.
1043

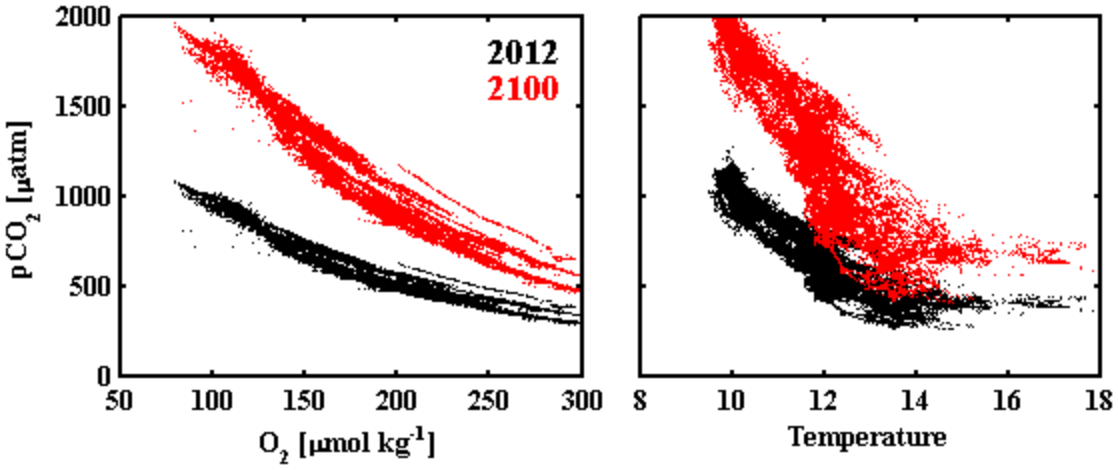

1044

1045 Figure 15: pCO_2 as a function of O_2 (left) and temperature (right) from the kelp forest and shelf
1046 break. Data observed in 2012 and projected for 2100 are plotted.
1047

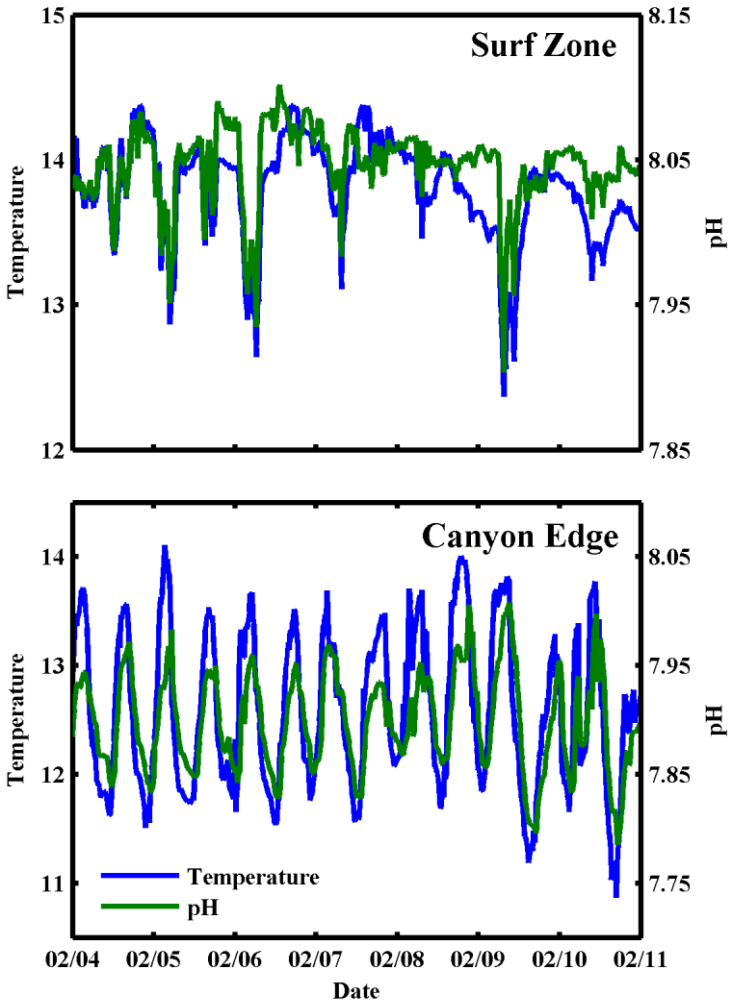

Supplementary Figure 1: Week long time series of temperature and pH at the surf zone (top) and canyon edge (bottom).